DMD Fast Forward. Published on October 11, 2007 as doi:10.1124/dmd.107.015321

DMD #15321

Permeability, Transport, and Metabolism of Solutes in Caco-2 Cell Monolayers: A Theoretical Study

Huadong Sun and K. Sandy Pang

Department of Pharmaceutical Sciences, Leslie Dan Faculty of Pharmacy,

University of Toronto, Toronto, Canada M5S 3M2

DMD Fast Forward. Published on October 11, 2007 as DOI: 10.1124/dmd.107.015321
This article has not been copyedited and formatted. The final version may differ from this version.

Running title page

Running title: Permeability, transport and metabolism in Caco-2

Corresponding author: Dr. K. Sandy Pang
Faculty of Pharmacy
University of Toronto
144 College Street
Toronto ON
Canada M5S 3M2
Tel: 416-978-6164
Fax: 416-978-8511
E-mail: ks.pang@utoronto.ca

Abstract: 250 words; 1 page

Introduction: 664 words

Discussion: 1391 words

Tables: 6

Figures: 18

References: 40

Abbreviations: Pgp, P-glycoprotein; P_{app}, effective permeability; EfR, efflux ratio; $CL_{int,sec}$, intrinsic clearance for apical efflux, mediated by transporters; $CL_{int,met}$, metabolic intrinsic clearance; CL_{abs}, intrinsic clearance for apical absorption, mediated by transporters; CL_{influx} and CL_{efflux}, intrinsic clearances for basolateral influx and efflux, respectively, mediated by transporters; CL_d, passive diffusion clearance common across apical and basolateral membranes; CL_{d4} and CL_{d1}, passive diffusion clearance from the apical and basolateral compartments into the cell compartment, respectively; CL_{d3} and CL_{d2}, passive diffusion clearance from the cell compartment into the apical and basolateral compartments, respectively; P_c, J_c and J_{max}, the permeability, flux, and apparent V_{max} estimated for the carrier system, respectively; K'_m and K''_m are the apparent K_ms estimated from the Eadie-Hofstee plot, with and without the Hill coefficient, respectively; f_{met}, fraction of dose metabolized

DMD Fast Forward. Published on October 11, 2007 as DOI: 10.1124/dmd.107.015321
This article has not been copyedited and formatted. The final version may differ from this version.

ABSTRACT

We explored the properties of a catenary model that includes the basolateral (B), apical (A), and cellular compartments via simulations under linear and nonlinear conditions to understand the asymmetric observations arising from transporters, enzymes, and permeability in Caco-2 cells. The efflux ratio (EfR, $P_{app,B\rightarrow A}/P_{app,A\rightarrow B}$), obtained from the effective permeability from the A→B or B→A direction under linear conditions, was unity for passively permeable drugs whose transport does not involve transporters; the value was unaffected by cellular binding or metabolism, but increased with apical efflux. Metabolism was asymmetric, showing lesser metabolite accrual for the B→A than A→B direction because of inherent differences in the volumes for A and B. Moreover, the net flux (total – passive permeation) due to saturable apical efflux, absorption, or metabolism showed nonconformity to simple Michaelis-Menten kinetics against $C_{D,0}$, the loading donor concentration. EfRs values differed with saturable apical efflux and metabolism (>1), and apical absorption (EfRs <1), but approached unity with high passive diffusive clearance (CL_d) and increasing $C_{D,0}$ at higher degree of saturation of the process. The J_{max} and K'_m [or the K''_m based on a modified equation with the Hill coefficient (β)] estimates from the Eadie-Hofstee plot revealed spurious correlations with the assigned V_{max} and K_m. The sampling time, CL_d, and parameter space of K_m and V_{max} strongly influenced both the correlation and accuracy of estimates. Improved correlation was found for compounds with high CL_d. These observations showed that the catenary model is appropriate in the description of transport and metabolic data in Caco-2 cells.

DMD Fast Forward. Published on October 11, 2007 as DOI: 10.1124/dmd.107.015321
This article has not been copyedited and formatted. The final version may differ from this version.

INTRODUCTION

The majority of drugs available in the market are oral dosage forms. For the assessment of permeability and oral drug absorption, *in silico* models (Stenberg et al., 2001) and high throughput systems such as the parallel artificial membrane permeability assay (PAMPA) (Kansy et al., 1998) and cell-based systems (Hidalgo et al., 1989) exist to relate drug permeability to absorption, especially for compounds that do not undergo intestinal metabolism (Usansky and Sinko, 2005). The most popular, high-throughput screening tool for drug permeability is the human colon carcinoma (Caco-2) (Hidalgo et al., 1989) or transfected Madin-Darby canine kidney (MDCKII) (Irvine et al., 1999) cells. Upon culture, Caco-2 cells differentiate and become confluent to form monolayers with tight junctions and polarized apical/mucosal (A side) and basolateral/serosal (B side) membranes that are structurally and functionally similar to those of enterocytes.

ABC efflux transporters such as P-glycoprotein (Pgp or MDR1, multidrug resistance associated protein 1), the multi-drug resistance-associated protein 2 (MRP2), and the breast cancer resistant protein (BCRP) are expressed on the mucosal membrane of Caco-2 (Hunter et al., 1993; Hirohashi et al., 2000), as are the absorptive transporters, such as the proton-coupled oligopeptide transporter (PEPT1) (Guo et al., 1999) and organic anion transporting polypeptide (OATP 2B1) (Kobayashi et al., 2003). Similarly, on the serosal membrane, basolateral efflux transporters, such as MRP3 (Hirohashi et al., 2000), and OSTα-OSTβ (Okuwaki et al., 2007) are expressed in Caco-2. In addition, multiple metabolic enzymes such as the sulfotransferases (SULTs), UDP-glucuronosyltransferases (UGTs) (Sun et al., unpublished data), and the glutathione S-transferases (GSTs) (Peters and Roelofs, 1989) reside in the Caco-2 cell monolayer. Besides, the cytochrome P450 3A4 (CYP3A4), which is inherently poorly expressed in cell monolayer, may be induced by incubation with 1α,25-dihydroxyvitamin D_3 or acquired by transfection of the CYP3A4 gene (Cummins et al., 2001). The Caco-2 system allows for paracelluar transport (Adson et al., 1994), and Ca^{2+}-Mg^{2+} free buffer has often been used to disrupt paracellular transport of fluorescein,

a highly fluorescent probe, for assessment of the contribution of the pathway (Troutman and Thakker, 2003a). Furthermore, an unstirred water layer that can impede the transport of highly lipophilic drugs has been described for the Caco-2 cells (Hildalgo et al., 1991).

Cell-based permeability models have become a necessary strategy in the drug discovery paradigm (Lentz et al., 2000; Polli et al., 2001). The protocol facilitates the drug-discovery scenario to define whether or not new drug entities are Pgp substrates. Inhibitors such as GF120918 are used to identify Pgp involvement and obliterate apical efflux. In parallel, computational models have evolved to describe Caco-2 transport. However, most of the interpretations express simplified views and provide approximate solutions for the passive permeability coefficient, P_{app}, by assuming that the system is a single barrier. Even for nonlinear cases, influx or efflux at the apical membrane was simplified by viewing the system as a single barrier and assuming that drug molecules present at either the apical or basolateral compartment have direct access to intracellular enzymes or efflux transporters (Guo et al., 1999; Williams et al., 2002; Troutman and Thakker 2003b, Tran et al., 2004).

We are of the view that the single barrier model for the Caco-2 cell monolayer is inadequate, and that a catenary model comprising basolateral (B), apical (A), and cellular compartments (Ito et al., 1999; Tam et al., 2003; Irie et al., 2004; González-Alverez et al., 2005) is more appropriate than what routine analyses subscribe, especially under nonlinear conditions. Given the importance of the Caco-2 system in drug discovery and development, we explored properties of the catenary model to gain a mechanistically-based understanding of the asymmetric observations arising from transporters, enzymes, and effective permeability under both linear and nonlinear conditions. We examined the definition of P_{app} under sink and non-sink conditions, and when the parameter was based on cumulative or timed-sampling. The definition of EfR and its dependence on transport, binding, and metabolic parameters was studied. Moreover, the appropriateness of estimates of Michaelis-Menten parameters, V_{max} (as J_{max}) and K_m (as K'_m or K''_m) was investigated.

DMD Fast Forward. Published on October 11, 2007 as DOI: 10.1124/dmd.107.015321
This article has not been copyedited and formatted. The final version may differ from this version.

THEORY

The Caco-2 Cell Model

We hereby briefly revisit the terminologies and concepts. Although we refer our terminology to the Caco-2 system, the kinetics derived may also apply to transfected cell lines or other similar, in vitro systems. The test compound is administered into the donor side, the apical (A) or basolateral (B) compartment, and samples are withdrawn at the alternate site (receiver side). Both "sink" and "non-sink" conditions for the Caco-2 system have been considered. "Sink" conditions refer to the situation in which back diffusion of drug in the receiver side to cell monolayer is negligible. Sink condition would be satisfied when the sampling is conducted within the time interval that drug concentration in the receiver side remain < 10% of the loading concentration, $C_{D,0}$ (Troutman and Thakker, 2003a) or when drug in the serosal side is removed rapidly and irreversibly, leaving no chance for the drug to return back to the enterocyte. In contrast, no assumption needs to be made for "non-sink" conditions; there is no need to assume that drug concentrations are maintained high in the donor side but low in the receiver side, and that drug molecules in receiver side do not re-enter the cell compartment.

Definition of P_{app} and EfR

The most common approach is to document drug appearance in receiver side. This permeability term, P_{app}, defined in Eq. 1, is commonly known as the apparent or effective permeability (Hilgers et al., 1990),

$$P_{app} = \frac{(\Delta A_R / \Delta t)/S}{C_{D,0}} \qquad (1)$$

where $(\Delta A_R/\Delta t)$ is the rate of drug appearance in receiver side, S is the surface area of the transwell (4.71 cm^2; Yamaguchi et al., 2000), and $C_{D,0}$ is the initial drug concentration in the donor side at time = 0. When the value is based on cumulative sampling (total amount transported from time = 0 up to the last sampling point), the cumulative P_{app} is obtained. However, when the value is based on

DMD Fast Forward. Published on October 11, 2007 as DOI: 10.1124/dmd.107.015321
This article has not been copyedited and formatted. The final version may differ from this version.

sampling at various time intervals, the incremental P_{app} is obtained, and $C_{D,0}$ now denotes the donor concentration at the onset of the time interval (Youdim et al., 2003). Permeability, when based in absence of transporters, denotes the ability of the molecule to traverse membranes by passive means. However, high passive permeability is not synonymous with high lipophilicity since hydrogen bonding or the presence of unstirred water layer for this group of compounds can delimit permeability to such an extent that the compounds would exhibit a low permeability.

Usually, the purpose of transport studies in Caco-2 monolayer is to ascertain whether or not the test compound is a substrate of the efflux transporter, especially Pgp. The efflux ratio (EfR), or ratio of effective permeability for a drug given into B to appear in A (B→A) direction to that in A→B direction (Eq. 2), is used.

$$\mathbf{EfR} = \frac{P_{\mathbf{app,B\rightarrow A}}}{P_{\mathbf{app,A\rightarrow B}}} \qquad (2)$$

Generally speaking, a value of < 1.2 or 1.5 for EfR infers that only passive diffusion is involved in drug transport, whereas EfR values that greatly exceed unity suggest that test compounds are substrates of efflux transporters at the apical membrane (Lentz et al., 2000; Polli et al., 2001). However, the inference is less certain for highly permeable substrates, even though the compounds are Pgp substrates; rapid influx of drugs by passive diffusion or active uptake transporters on apical membrane can overcome the effect of apical efflux (Lentz et al., 2000).

For EfR values falling between 1~1.5, there exists the dilemma to identify whether or not the test compound is a substrate of Pgp or other efflux transporters. Methods involving use of inhibitors are thus developed. The effective permeability (P_{app}) in the presence of the specific inhibitors, GF120918 for Pgp and BCRP (den Ouden et al., 1996), Ko143 for BCRP (Allen et al., 2002), and MK571 for the MRPs (Gekeler et al., 1995), would be reduced to approximate values of the passive permeability (P_{PD}) when the transporter component is drastically reduced or totally obliterated. To

DMD Fast Forward. Published on October 11, 2007 as DOI: 10.1124/dmd.107.015321
This article has not been copyedited and formatted. The final version may differ from this version.

avoid ambiguity in the definition of the concentration employed, the inhibitor should be added to both A and B compartments.

The absorptive quotient (AQ) (Eq. 3) and the secretory quotient (SQ) (Eq. 4) are introduced with administration of the inhibitor into the apical and basolateral sides (Troutman and Thakker, 2003c). These expressions are derived from P_{app} in absence and presence ($P_{PD,A\rightarrow B}$ or $P_{PD,B\rightarrow A}$) of inhibition.

$$AQ = \frac{P_{PD,A\rightarrow B} - P_{app,A\rightarrow B}}{P_{PD,A\rightarrow B}} \quad (3)$$

$$SQ = \frac{P_{app,B\rightarrow A} - P_{PD,B\rightarrow A}}{P_{PD,B\rightarrow A}} \quad (4)$$

A change in P_{app} with inhibitors would alter the AQ and SQ values if apical efflux transporters are involved. The enhancement of the asymmetric transport of drugs in A→B (absorptive) direction with attenuation of transport in B→A (secretory) direction with Pgp inhibitors suggests that Pgp is involved in drug transport. The unidirectional measurements of AQ or SQ would reduce the workload in drug screening while providing reliability to bidirectional study for identification of Pgp substrates. It has been proposed that, if the AQ or SQ value is more than 0.3, the drug is considered to be a Pgp substrate (Thiel-Demby et al., 2004).

Caco-2 Cells and Enzymes. Caco-2 also houses various drug metabolizing enzymes, and the system has been used to study drug metabolism as well as the interplay between transporters and enzymes (Cummins et al., 2001). Metabolism in Caco-2 monolayer could modulate P_{app}, EfR, and net efflux rates. The effects of metabolism have not been properly addressed.

Various laboratories have used different terminologies to express the cellular metabolism within the Caco-2 cells system. One of these is the extraction ratio (ER), given by the ratio of the total amount of the metabolite (Met_{total}) divided by the sum of the Met_{total} and the drug amount(s) in the receiving compartment (D_R) in Eq. 5 (Fisher et al., 1999), or by the sum of Met_{total}, D_R and the drug amount(s) in the cell (D_{cell}) (Eq. 6) (Cummins et al., 2001).

DMD Fast Forward. Published on October 11, 2007 as DOI: 10.1124/dmd.107.015321
This article has not been copyedited and formatted. The final version may differ from this version.

$$ER = \frac{Met_{total}}{Met_{total} + D_R} \quad (5)$$

$$ER = \frac{Met_{total}}{Met_{total} + D_R + D_{Cell}} \quad (6)$$

These equations on the extraction ratio, ER, have been misconstrued to describe the extents of metabolism since the equations have neglected to consider the entire mass of the system, namely, drug in the donor and/or cell compartments also equilibrates in the system. The above equations have led to the misconception that metabolism can be increased with increase in efflux transport under linear conditions. A simple equation (Eq. 7) that describes the fraction of dose metabolized (f_{met}) has been used to correct for the misconception (Tam et al., 2003).

$$f_{met} = \frac{Met_{total}}{C_{D,0} \times V_D} = \frac{Met_{total}}{dose} = \frac{Met_{total}}{Met_{total} + D_R + D_D + D_{cell}} \quad (7)$$

The parameter, f_{met}, expressed as a fraction of dose, reflects the metabolic efficiency of the monolayer system and is more appropriate to describe the extent of drug metabolism in Caco-2 monolayer.

***Nonlinearity*.** In order to understand the transport mechanism of drugs across Caco-2 monolayer, the individual contribution of passive diffusion/permeability (P_{PD}) and transporters (P_c) to the overall or total permeability (P_{app}) has to be distinguished under nonlinear situations. The carrier-mediated permeability (P_c), has been defined as $J_{max}/(K'_m + C_{D,0})$ and J_{max}/K'_m for nonlinear and linear cases, respectively (Troutman et al., 2003b).

$$P_c = \left| P_{app} - P_{PD} \right| = \frac{J_{max} / S}{K'_m + C_{D,0}} \; or \; \frac{J_{max} / S}{K'_m} \quad (8)$$

K'_m and J_{max} are estimates of the Michaelis-Menten constant (K_m) and maximum flux (V_{max}) for the transporter, respectively. Usually, P_c, or the carrier-mediated permeability associated with the saturable process, is estimated from Eq. 8 as ($P_{app} - P_{PD}$). In the case of saturable apical efflux, P_{PD} may be evaluated from use of inhibitors of efflux transporters. The apical, absorptive transporter or

DMD Fast Forward. Published on October 11, 2007 as DOI: 10.1124/dmd.107.015321
This article has not been copyedited and formatted. The final version may differ from this version.

enzyme activity is usually negligible in non-transfectants (Caco-2 cells), and transporter/metabolic activity shows up only in transfectants. Thus, P_{app} may be evaluated from transfectants, and P_{PD}, from mock-transfected Caco-2 cells (Bhardwaj et al., 2005; Cummins et al., 2001). Thus P_c may be obtained from difference.

Analogously, the net flux due to carrier-mediated transport (J_c) is viewed as the difference between the total flux (J) and flux due to passive diffusion (J_m), and was estimated as $P_c SC_{D,0}$. These relate to the estimated parameters, J_{max} (for V_{max}) and K'_m (for K_m). In most of the investigations, it has been assumed that apical efflux is the saturable process and that substrate concentration at the vicinity of the transport process is the initial loading concentration, $C_{D,0}$.

$$J_c = \left| J - J_m \right| = \frac{J_{max}}{K'_m + C_{D,0}} C_{D,0} \qquad (9)$$

The strategies taken involved plotting J_c vs. $C_{D,0}$ in the Eadie Hofstee plot for the appraisal of J_{max} and K'_m (Troutman and Thakker, 2003b). More often than not, curvature was observed in the plot of J_c vs. $C_{D,0}$, since $C_{D,0}$ is not the substrate concentration and the Caco-2 system is not a single barrier. To improve the fit, a Hill number or coefficient, β, suggestive as an estimate of the number of binding sites on the transporter, was added into the Eq. 10 (Stephens et al., 2001).

$$J_c = \frac{J_{max}}{K''^{\beta}_m + C^{\beta}_{D,0}} C^{\beta}_{D,0} \qquad (10)$$

The equation was re-arranged as shown below.

$$\log\left\{\frac{J_{max}}{J_c} - 1\right\} = -\beta \log C_{D,0} + \beta \log K''_m \qquad (11)$$

In this "improvised method", J_{max} was first estimated from the Y-intercept of the Eadie-Hofstee plot, and β and K''_m were estimated from refitting of data to Eq. 11.

DMD Fast Forward. Published on October 11, 2007 as DOI: 10.1124/dmd.107.015321
This article has not been copyedited and formatted. The final version may differ from this version.

METHODS

The Catenary Caco-2 Cell Model

A catenary model, similar to those used by others (Ito et al., 1999; Tam et al., 2003; Irie et al., 2004; González-Alvarez et al., 2005), was employed to appraise various aspects of the effective permeability, efflux ratio, and data interpretation on transporters and enzymes in Caco-2 monolayers. The model comprised the absorptive and ABC-transporters of the apical membrane and influx and efflux barriers at the basolateral membrane as two sets of potential barriers. The complexity of housing the ABC-transporters in a lipid bilayer was not considered (Tran et al. 2005), since the equilibrium of drug molecules between the aqueous compartment and inner/outer plasma membrane would be achieved rapidly. Also, paracellular transport was neglected, as this could be embedded in the parameter for passive diffusion permeability.

The cell monolayer is viewed as a system that includes transporters and enzymes and allows for drug diffusion and cellular binding. The net flux associated with drug permeation in the catenary model involves two different barriers, one at the apical membrane separating the apical compartment and cell, and the other at the basolateral membrane, separating the basolateral compartment and cell (Fig. 1). The terms CL_{abs} and CL_{d4} denote the absorptive clearance ascribed to transporter-mediation and passive diffusion on the apical membrane, respectively; $CL_{int,sec}$ and CL_{d3} denote the secretory and passive transport clearances of drug from the cell back to the apical compartment, respectively; CL_{d1} and CL_{influx} represent the passive and transporter-mediated influx clearances of drug between the basolateral compartment and cell monolayer, respectively; CL_{d2} and CL_{efflux} represent the passive and transporter-mediated efflux clearances of drug between cell monolayer and the basolateral compartment, respectively. Unless specified, it was assumed that the clearances driven by passive diffusion are equal ($CL_{d1} = CL_{d2} = CL_{d3} = CL_{d4} = CL_d$). These CL_d terms relate to drug permeability by passive diffusion. A drug with high CL_d is highly permeable whereas a drug with low CL_d is poorly permeable and requires transporters to facilitate transport.

DMD Fast Forward. Published on October 11, 2007 as DOI: 10.1124/dmd.107.015321
This article has not been copyedited and formatted. The final version may differ from this version.

In this study, simulations were conducted to produce profiles on transport and metabolism of solutes in the Caco-2 monolayer that was grown on a transwell of insert diameter 24 mm (6-well plate). V_{ap} (1.5 ml) and V_{baso} (2.5 ml) were the volumes of buffer solution in the apical and basolateral compartments, respectively. One popular approach to estimate the cellular volume (V_{cell}) is by geometrical calculation, in which V_{cell} equals the insert area x cell height. Blais et al. (1987) had measured the cell height by a pulse height analyzer and estimated V_{cell} to be 3.66 µl/mg protein. Since the protein content of a confluent Caco-2 monolayer was 3 mg (Irie et al., 2004), the V_{cell} was calculated to be 10.98 µl (3.66 µl/mg x 3 mg). In the second method, Yamaguchi et al. (2000) studied sulfanilamide, a poorly protein-bound compound whose transport was mediated only by passive diffusion, and estimated V_{cell} to be 12.15 µl from the amount of sulfanilamide cumulated in the cell monolayer/external sulfanilamide concentration, at equilibrium. Hence, in the present study, we took the average value of these V_{cell} values, 11.56 µl, for all simulations.

Under nonlinear conditions, the rate of solute appearance in the receiver side changed with the initial concentration in the donor side, $C_{D,0}$. These changes with concentration were observed with saturation of the apical efflux (Gonzáelz-Alverez et al., 2005), apical influx (Tamai et al., 1997), basolateral influx (Irie et al., 2004) or metabolism (Sun et al., unpublished data). The linear model described in Fig. 1 was modified to include non-linearity by substitution of the clearance term of the apical or basolateral membrane with $V_{max}/(K_m + C_u)$, where C_u was the unbound drug concentration, and V_{max} and K_m were the maximum velocity and Michaelis-Menten constant, respectively.

For simplicity, metabolism within the system was viewed as the aggregate amount of metabolite formed (Met) that was associated with the metabolic intrinsic clearance, $CL_{int,met}$. Drug binding to proteins in the apical and basolateral compartments would occur due to the presence of sloughed-off mucosal cells (unbound fractions, f_{ap} and f_{baso}, respectively), and within the cell (unbound fraction, f_{cell}). Binding would affect the mass transfer and metabolic rates that are based on unbound drug concentrations. The assumption that formed metabolites did not compete with the

parent drug for the transporters, enzymes, and drug-protein binding was made. The substrate was further assumed to undergo simple Michaelis-Menten kinetics for both transport and metabolism under nonlinear conditions.

Solutions and Simulations

Mass balance equations (see appendix) based on the catenary model shown in Fig. 1 were developed. Under linear condition, the equations were solved for P_{app} and EfR with the program, Maple 9.0 (Waterloo Maple Inc., Waterloo, Canada). Computer simulations were performed under linear and nonlinear conditions with Scientist (Micromath®, Salt Lake City, Utah). Different CL_d, $CL_{int,met}$, CL_{abs}, $CL_{int,sec}$, and V_{max} and K_m were assigned.

DMD Fast Forward. Published on October 11, 2007 as DOI: 10.1124/dmd.107.015321
This article has not been copyedited and formatted. The final version may differ from this version.

RESULTS

Linear Conditions

Both sink and non-sink conditions were examined. The P_{app} under non-sink conditions was best to describe drug transport, and the incremental P_{app}, estimated at different time intervals was less stable than the cumulative P_{app} (based on amount transported/time zero to time of sampling) in the description of EfR (data not shown). Hence, further analyses only pertained to the cumulative P_{app}. Although an explicit solution was found for P_{app} by matrix inversion for non-sink conditions, the solution was not readily presentable because the expression was very lengthy. Instead, computer simulation was used to show patterns of P_{app} and the factors that modulated P_{app}.

P_{app} and EfR, in Absence of Metabolic Enzyme and Transporter Activity. When transporter and enzyme activities were absent, P_{app} was found to be time- and permeability-dependent (Fig. 2). With the assumption that $CL_d = CL_{d2} = CL_{d3} = CL_{d4} = CL_d$, $P_{app,\,A\rightarrow B}$ and $P_{app,\,B\rightarrow A}$ profiles were found to be identical (Fig. 2), resulting in EfR values that were constant (unity) and time-invariant. Binding within the cell further affected the P_{app} patterns (Fig. 2, insets), rendering decreased P_{app} with decreasing unbound fraction, f_{cell}. However, binding would not alter EfR, as predicted by Eq. 12 below.

P_{app} and EfR in Presence of Efflux or Metabolism. P_{app} was found to be modulated by $CL_{int,sec}$ (Fig. 3) at both high and low passive diffusion clearance, CL_d. $P_{app,B\rightarrow A}$ was increased while $P_{app,A\rightarrow B}$ was decreased with increasing $CL_{int,sec}$; thus EfRs were increased, and the values were higher for drugs with low CL_d (Fig. 3). By contrast, P_{app} values were identical in both absorptive and secretory directions, and P_{app} decreased with increasing $CL_{int,met}$ (Fig. 4); the P_{app} values were lower for drugs of lower CL_d. Values of the resultant EfR converged at unity, regardless of values of $CL_{int,met}$, and were not affected by metabolism.

DMD Fast Forward. Published on October 11, 2007 as DOI: 10.1124/dmd.107.015321
This article has not been copyedited and formatted. The final version may differ from this version.

Solution for EfR. The solution of EfR existed in a concise form under linear conditions, and was similar to that reported by Adachi et al. (2001), with the exception of the unbound fractions.

$$\mathrm{EfR} = \frac{f_{baso}(CL_{d1} + CL_{influx})(CL_{int,sec} + CL_{d3})}{f_{ap}(CL_{d2} + CL_{efflux})(CL_{abs} + CL_{d4})} \quad (12)$$

$CL_{int,met}$ and f_{cell} were absent in Eq. 12 for EfR. The equation implied that, under linear condition, intracellular metabolism and the binding of drugs to intracellular protein would not influence EfR. When protein was absent ($f_{ap} = f_{baso} = 1$) or when binding was similar ($f_{ap} = f_{baso}$), the binding terms would disappear, and the f_{baso} and f_{ap} terms were canceled, and Eq. 12 was further simplified:

$$\mathrm{EfR} = \frac{(CL_{d1} + CL_{influx})(CL_{int,sec} + CL_{d3})}{(CL_{d2} + CL_{efflux})(CL_{abs} + CL_{d4})} \quad (13)$$

Based on Eq. 13, the effect of the various clearances on EfR was investigated. The results are summarized in three-dimensional graphical presentations. As shown in Fig. 5A, values of EfR fell between 1 and 2 when the test compounds were of high CL_d (~ 1 ml/min), even when the efflux transporter activity ($CL_{int,sec}$) was substantial (0.8 ml/min). The same was observed for compounds that were actively taken up by the apical transporters ($CL_{abs} >> CL_{d4}$), rendering values of EfR below unity (Fig. 5B). However, extremely high EfR values would result with increasing $CL_{int,sec}$ but decreasing CL_d (Fig. 5A) or CL_{abs} (Fig. 5B) that disallowed rapid equilibration of drug between the cellular and the apical compartment. By contrast, decreasing values of CL_{influx}/CL_{efflux} would furnish modest values of EfR (between 0.5 and 2) even for substrates that were readily effluxed out at the apical membrane ($CL_{int,sec}$ = 0.9 ml/min) (Fig. 5C).

With the assumption that CL_{d1} equals CL_{d2}, CL_{d3} equals CL_{d4} and only apical efflux is carrier-mediated (i.e., $CL_{abs} = CL_{influx} = CL_{efflux} = 0$), Eq. 13 was further simplified,

$$\mathrm{EfR} = 1 + \frac{CL_{int,sec}}{CL_{d4}} \quad (14)$$

Eq. 14 inferred that, EfR was dependent on the relative magnitude of $CL_{int,sec}$ and CL_{d4} in absence of transporter-mediated apical influx, basolateral influx and efflux. For a Pgp substrate such as verapmil

DMD Fast Forward. Published on October 11, 2007 as DOI: 10.1124/dmd.107.015321
This article has not been copyedited and formatted. The final version may differ from this version.

that has a high CL_d, $CL_{int,sec} \sim CL_d$ and the efflux ratio was close to 2. For other drugs of low CL_d that are Pgp substrates ($CL_{int,sec} > CL_d$), EfR was disproportionately higher (Lentz et al., 2000; Polli et al., 2001). Fortunately, the ambiguity may be removed with use of potent Pgp inhibitors that would drastically reduce the EfR, revealing AQ and SQ values that denote Pgp transport. Therefore, EfR values needed to be appraised and compared, together with other permeability data with Pgp inhibitors, such as AQ and SQ.

Asymmetry of Metabolism. The amount of metabolite formed (Met_{total}) was normalized to the dose, and expressed as f_{met} (Eq. 7). A faster metabolite formation rate was observed with apical over basolateral dosing, even with identical initial concentration administered. The observed asymmetry in metabolism resulting from administration into the apical or basolateral side was expected because of differences in volumes (V_{ap} and V_{baso}). When identical permeability clearances existed across the apical and basolateral membranes ($CL_{d1} = CL_{d2} = CL_{d3} = CL_{d4}$) and carrier-mediated transport was absent ($CL_{abs} = CL_{int,sec} = CL_{influx} = CL_{efflux} = 0$), $f_{met\ B\rightarrow A}$ /$f_{met\ A\rightarrow B}$ was less than 1 (Fig. 6). When V_{ap} and V_{baso} were set up to be equal, the metabolic asymmetry disappeared (simulation not shown). With increasing incubation time, $f_{met\ A\rightarrow B,}$ $f_{met\ B\rightarrow A}$, and $f_{met\ B\rightarrow A}$ /$f_{met\ A\rightarrow B}$ increased and finally approached 1 (when time approached infinity in this system, all drug ultimately became metabolized and f_{met} in both directions equaled unity). Again, the passive diffusion clearance (CL_d) was important, and a greater permeability of the solute facilitated a faster entry of drug for cellular metabolism (cf. Figs. 6A and 6B). Carrier-mediated efflux on the apical side ($CL_{int,sec}$) decreased values of $f_{met,B\rightarrow A}$ and $f_{met,A\rightarrow B}$ by removing cellular substrate for metabolism, and also affected the value of $f_{met,B\rightarrow A}/f_{met,A\rightarrow B}$, accentuating the asymmetry observed for metabolite formation.

Nonlinear Conditions

Saturable terms, V_{max} and K_m, were used as replacement of the intrinsic clearances in the catenary model (Fig. 1); CL_{d1}, CL_{d2}, CL_{d3}, and CL_{d4}, were set equal to CL_d, with the unbound fractions were set to unity. For each simulation, only one saturable process (apical influx or efflux,

DMD Fast Forward. Published on October 11, 2007 as DOI: 10.1124/dmd.107.015321
This article has not been copyedited and formatted. The final version may differ from this version.

basolateral influx or efflux, or intracellular metabolism) was considered in the Caco-2 system. Simulations were then performed to provide data for appraisal of the appropriateness of the estimates (K'_m or K''_m and J_{max}) vs. the assigned K_m and V_{max} for the saturable process. The strategy generated sets of data with assigned constants (K_m and V_{max}, CL_d and $C_{D,0}$) and these were further manipulated into forms used in data interpretation. The true values and the derived estimates were then compared.

First, the manner in which saturation of apical efflux transporters affected P_{app} and EfR at increasing $C_{D,0}$ was examined. Solutes with high CL_d entered the cell compartment rapidly and readily saturated apical efflux with increasing $C_{D,0}$. Values of $P_{app,\ A\rightarrow B}$ increased with $C_{D,0}$ (Fig. 7, top panel), whereas $P_{app,\ B\rightarrow A}$ decreased with $C_{D,0}$ (Fig. 7, middle panel). These resulted in attenuated EfR´s (Fig. 7, bottom panel). By contrast, less changes for $P_{app,\ A\rightarrow B}$ and $P_{app,\ B\rightarrow A}$ were found for drugs of low CL_d since these failed to enter the cell readily to saturate apical efflux transporters. Second, the effect of saturable apical efflux on metabolism was considered. The presence of apical efflux reduced the fraction of dose metabolized, f_{met}, since efflux was competing with metabolism. An increase in V_{max} for apical efflux also reduced f_{met}, regardless of whether the drug was given into A or B, and this existed when the drug equilibrated rapidly (Fig. 8A) or slowly (Fig. 8B).

Eadie-Hofstee Plot. Characteristic profiles were obtained upon plotting P_c (Eq. 8) and J_c (Eq. 9) against $C_{D,0}$ (Figs. 9A and 9B) when saturable efflux existed. A lack of conformity to linearity was commonly observed with the Eadie-Hofstee plot for the estimation of K'_m and J_{max} (flux vs. flux/$C_{D,0}$) (Fig.9C). Usually, the intercept and slope of the plot associated with the straight line component would be used for estimation of the J_{max} and K'_m, respectively (see straight line in inset, Fig. 9C, for drug of high CL_d). Poor estimates would result when curvature existed in the Eadie-Hofstee plot for solutes of low CL_d (< 1 ml/min). When Eq. 10 was used to improve the fit with the Hill coefficient, β, K''_m, estimated from refitting of data to Eq. 11, was not much improved compared to K'_m (see below). The estimate of J_{max} remained unchanged since the parameter was estimated from the Y-intercept of the Eadie-Hofstee plot.

DMD Fast Forward. Published on October 11, 2007 as DOI: 10.1124/dmd.107.015321
This article has not been copyedited and formatted. The final version may differ from this version.

Estimation of Parameters: Non-linear Apical Efflux. With varying CL_d (0.01, 0.1, or 1 ml/min), further simulations were performed with varying V_{max} (0.05 to 50 nmol/min) at a fixed K_m (0.5 μM) for apical efflux. The simulations were repeated by changing the K_m (0.5 to 50 μM) at a fixed V_{max} (0.5 nmol/min) to arrive at different sets of J_c at varying sampling times (0 to 120 min). The plots P_c, the carrier-mediated flux (J_c), and the Eadie-Hofstee plot vs.$C_{D,0}$ (Figs. 9A to 9C) revealed that CL_d strongly influenced the curvature of the Eadie-Hofstee plot with time. Higher values of P_c and J_c were obtained for the B→A than the A→B direction, yielding asymmetric J_{max} and lower K'_m estimates (Tables 1 and 2). The early data points of the Eadie-Hofstee plots were used to estimate the J_{max}, and K'_m from the intercept and slope, respectively (Fig. 9C). A linear relationship was observed for the Eadie-Hofstee plot only with higher CL_d (Fig. 9C, see inset). Upon presenting the entire set of estimates, it was apparent that J_{max} differed from the assigned V_{max} and varied according to the value of CL_d (Fig. 10, Table 1). The correlation was poor at low CL_d (0.01 ml/min), whereas an improved and linear correlation was identified at increasing CL_d ($\geq$ 1 ml/min) (Figs. 10A to 10C). The estimated K'_m and K''_m were less affected by CL_d. Linear relationships were found between K'_m and K''_m and the assigned K_m (Figs. 10D to 10F); the values became closest when CL_d was highest (Table 2). However, no further improvement was provided with use of Eq. 10 or 11 to arrive at K''_m (Table 2, Figs. 10D to 10F).

Estimation of Parameters: Non-Linear Apical Absorption. With varying CL_d (0.01, 0.1, or 1 ml/min), simulations were performed with varying V_{max} (0.05 to 50 nmol/min) but at a fixed K_m (0.5 μM), and at varying K_m (from 0.5 to 50 μM) but at a fixed V_{max} (0.5 nmol/min) for the apical absorption transporter to arrive at sets of P_c and J_c data (Fig. 11). With saturable apical absorption, higher P_c and J_c values were obtained in the B→A and not A→B direction, except for drugs of a very low CL_d (Figs. 11A and 11B). Again, curvatures were observed for the Eadie-Hofstee plot, except for drugs of high CL_d (see inset) (Fig. 11C). The estimated J_{max} was poorly correlated to the V_{max} especially when CL_d was lower (Figs. 12A to 12C; Table 3); but a linear correlation between J_{max} and

DMD Fast Forward. Published on October 11, 2007 as DOI: 10.1124/dmd.107.015321
This article has not been copyedited and formatted. The final version may differ from this version.

V_{max} was attained when CL_d values were high (Fig. 12C). The correlation between K'_m and K''_m to K_m was acceptable among the various CL_d (Figs. 12D to 12F; Table 4), and improved correlations existed when the CL_d values were high (Fig. 12F). Again, no further improvement was demonstrated with use of Eq. 10 or 11 to arrive at K''_m (Table 4, Figs. 12D to 12F).

Estimation of Parameters: Non-Linear Metabolism. With varying CL_d (0.01, 0.1, or 1 ml/min), simulations were performed, with varying V_{max} (0.05 to 50 nmol/min) at a fixed K_m (0.5 μM) for the metabolism, and at varying K_m (0.05 to 50 μM) at a fixed V_{max} (0.5 nmol/min), to arrive at sets of P_c and J_c data (Fig. 13). With saturable metabolism, values of P_c were higher with higher CL_d (Fig. 13A). Higher J_c values were observed in the A→B and not B→A direction (Fig. 13B), yielding correspondingly higher V_{max} (Y-intercept) (Fig. 13C). The correlation between J_{max} and V_{max} was poor regardless of values of CL_d (Fig. 14A to 14C; Table 5). By contrast, a linear correlation was found between K'_m and K''_m to K_m among the various CL_d (Fig. 14D to 14F; Table 6); the correlation improved when CL_d values were high. Again, no further improvement was provided with use of Eq. 10 or 11 to arrive at K''_m (Table 6, Fig. 14D to 14F).

Sampling Time. Sampling in the Caco-2 system was often performed at 1 or 2 h intervals. However, the manner in which sampling time affected the J_c estimates was seldom studied. We examined how sampling time affected estimation of P_c and J_c within the sets of simulations performed on saturation of apical efflux, apical absorption, and metabolism. Indeed, the sampling time affected values of J_c, although saturation profiles were retained vs. $C_{D,0}$ in both A→B and B→A (Fig. 15). Hence, the general shapes were retained for all of the Eadie-Hofstee plots, but estimates for K'_m and J_{max} would change when the sampling time, whether ½, 1 h or 2 h was used (data not shown).

Effect of Nonlinear Metabolite Formation. Simulation was performed to examine how the various saturable processes affected metabolite formation. For drugs of high CL_d (1 ml/min), saturable apical efflux (Fig. 16A), apical absorption (Fig. 16B), basolateral efflux, (Fig. 16C) and basolateral influx (Fig. 16D) resulted in asymmetric metabolite formation, namely, higher for the

DMD Fast Forward. Published on October 11, 2007 as DOI: 10.1124/dmd.107.015321
This article has not been copyedited and formatted. The final version may differ from this version.

secretory direction over the absorptive direction. The trend was partially due to the higher volume of the basolateral compartment; the dose ($V_{baso}C_{D,0}$) was larger than ($V_{ap}C_{D,0}$). Patterns for metabolite formation under saturable apical efflux (Fig. 16A) and basolateral efflux (Fig. 16C) were similar; lesser metabolism was observed with higher V_{max}'s to bring drug molecules out of the cell. The cumulative amount of metabolite formed was time-dependent (Fig. 16). Also, similar patterns existed between the profiles of metabolite formation for saturable absorption or basolateral influx: greater extents of metabolism were found associated with higher V_{max} since this tended to bring more drug molecules into the cell (Figs. 16B and 16D). For drugs of poor diffusion clearance (CL_d = 0.01 ml/min), greater amounts of metabolite formed were seen in the B→A direction, except when the apical transporter was present (Fig. 16F). At low CL_d, drug transport into and out of the cell would be nominal, unless there was enhanced apical absorption by transporters, rendering a greater extent of metabolism in the A→B direction; the trend intensified with increased V_{max} for the absorptive transporter (Fig. 16F).

When metabolite formation (at 1 h) was further examined at increasing $C_{D,0}$, trends indicating higher metabolite formation for the B→A direction over the A→B direction was unilaterally observed (Figs 17A to 17D), regardless of the saturable process: apical efflux, apical absorption, basolateral influx, or basolateral efflux. The cumulative amount of metabolite formed was less with higher V_{max} associated with saturable apical efflux (Fig. 17A) and saturable basolateral efflux (Fig. 17C), and opposite trends existed with saturation of apical absorption and basolateral influx (Figs. 17B and 17D). For drugs of poor diffusion clearance (CL_d = 0.01 ml/min), higher metabolite formation was again seen in the B→A direction, except when apical absorptive transport was present (Fig. 17F). At low CL_d, transport into and out of the cell would be nominal unless there was enhanced absorption by transporters, rendering more metabolism in the A→B direction. The trend intensified when the V_{max} for the absorptive transporter was increased (Fig. 17F).

DMD Fast Forward. Published on October 11, 2007 as DOI: 10.1124/dmd.107.015321
This article has not been copyedited and formatted. The final version may differ from this version.

Effect of Nonlinear Processes on EfR. Patterns of EfR under nonlinear conditions were examined. In these simulations, the saturable component was assigned a V_{max} of 0.5 nmol/min and K_m of 0.5 μM, and $CL_{d1} = CL_{d2} = CL_{d3} = CL_{d4} = CL_d$. EfRs values differed with saturable apical efflux and metabolism (>1), and apical absorption (EfRs <1), but approached unity with high CL_d and increasing $C_{D,0}$ at higher degree of saturation of the process. Saturable apical efflux (Fig. 18A) resulted in EfR values that exceeded unity, but approached unity at high $C_{D,0}$ when the apical efflux transporter was becoming saturated. Similar to the linear case, lower EfR values were found at higher CL_d. A reverse trend was observed for saturable apical influx, showing EfR values below unity (Fig. 18B). Increasingly higher EfRs resulted with higher CL_d and $C_{D,0}$. With saturable metabolism, an upswing then downswing pattern was observed for EfR with $C_{D,0}$, and the changes were more pronounced at higher CL_d (Fig. 18C). For saturable apical efflux, influx and metabolism, rapid drug entry by passive diffusion (high CL_d) counteracted the effects of the saturable process on EfR. Eventually, the EfR values return to unity when the apical efflux, absorptive or metabolic process failed to contribute significantly to the system with increasing $C_{D,0}$, as if only passive diffusion prevailed under linear conditions (Fig. 5 and Eq. 12).

Other Simulations. Other scenarios such as saturation of basolateral influx or basolateral efflux were not examined. This was because the patterns generated would be similar to those simulated for saturation of apical influx and apical secretion (mirror images for donor vs. receiver side) although minor differences would exist due to differences in volumes (V_{ap} and V_{baso}).

DMD Fast Forward. Published on October 11, 2007 as DOI: 10.1124/dmd.107.015321
This article has not been copyedited and formatted. The final version may differ from this version.

DISCUSSION

The Caco-2 system has become the gold standard to relate drug permeability to oral drug absorption (Hidalgo et al., 1989; Lentz et al., 2001; Polli et al., 2001; Thiel-Demby et al., 2004). Due to the prevalent use, a thorough examination in revisiting the terminologies used in literature and data interpretation in the Caco-2 monolayer is therefore justified. Eq. 1 was established under Fick's law to define drug permeability, P_{app}, with the assumptions that the driving force is the concentration gradient difference and that a single barrier exists for the Caco-2 monolayer (Hilgers et al., 1990). Although P_{app} is a time-dependent variable and higher P_{app} is associated with higher CL_d, the ratio of P_{app} ($P_{app,B\rightarrow A}/P_{app,A\rightarrow B}$) yields a meaningful EfR that is time-independent and CL_d-invariant (unity) when transporter activity is absent.

The meaning of EfR under linear condition was further clarified by Eq. 12. As shown in Eq. 12, EfR is dependent not only on the apical, secretory intrinsic clearance ($CL_{int,sec}$) but the relative magnitude of passive diffusion and transport clearances at the basolateral membrane (CL_{d1}+CL_{influx}) /(CL_{d2}+CL_{efflux}), CL_{d3} and CL_{d4}, and the apical absorptive clearance, CL_{abs}. Hence, the value of EfR may not always identify whether or not a test compound is a Pgp substrate. For drugs of rapid uptake clearances at the apical membranes, values of EfR are reduced by high CL_{d4} (Eq. 14) or CL_{abs} values (Fig. 5); the asymmetrical influx and efflux on basolateral membrane (CL_{influx}/CL_{efflux}) can also modulate the EfR. The same comment was made by Adachi et al. (2001). Even with the simplification that $CL_{abs} = 0$ and all diffusive clearances are identical ($CL_{d1} = CL_{d2} = CL_{d3} = CL_{d4}$), values of EfR may still hover around unity for drugs whose diffusion clearance (CL_{d4}) is high in relation to that of the secretory clearance (Eq. 14) (Lentz et al., 2000).

Also, EfR will be affected differentially by secretion and metabolism under linear conditions. Pgp-, BCRP- or MRP2-mediated efflux tends to provide higher EfR values when $CL_{int,sec} >> CL_d$ and when the passive diffusion clearance (CL_d) is low, rendering asymmetry in permeability from the B→A direction over the A→B direction (Fig. 3). For solutes of high CL_d, ambiguous EfR values

DMD Fast Forward. Published on October 11, 2007 as DOI: 10.1124/dmd.107.015321
This article has not been copyedited and formatted. The final version may differ from this version.

(close to unity) may result unless $CL_{int,sec}$ is extremely high (Fig. 3A). The possibility that the compound is a Pgp substrate needs to be clarified with use of inhibitors by the AQ and SQ (Eqs. 3 and 4). For solutes with low CL_d, higher EfR values will result as a consequence of secretion for Pgp substrates (Fig. 3B). By contrast, EfR is not affected by metabolism; the metabolic intrinsic clearance affects P_{app} in the B→A and A→B directions to the same extent, thereby EfR remains unchanged (Fig. 4). Extents of metabolite formation in A→B direction is higher than that in B→A direction; The pattern is inherently asymmetric simply because of unequal V_{ap} and V_{baso}, and metabolite formation is reduced by apical secretion in both directions (Fig. 6).

Saturation of transport and metabolic processes, however, will be encountered with increasing drug loading concentration within the Caco-2 cell system. The biggest disappointment in other existing data interpretation strategy lies in treating the Caco-2 cell system as a single barrier for parameter estimates of saturable processes. Even when perfect data for P_c and J_c are attainable with use of "specific" inhibitors that completely block the secretory process, or when transport/metabolic activities are associated only with transfected but not mock-transfected cells to enable precise measurements, the J_{max} and K'_m estimates are a far cry from the true values (Table 1 to 6). The method, based on the assumption that the Caco-2 cell system is a single barrier will yield inappropriate estimates.

In addition, the time of sampling (Fig. 15), the passive permeability of drug, tissue binding, metabolism, and the parameter space of K_m and V_{max} strongly influence both the correlation and accuracy of prediction. Saturation in apical absorption, efflux, or metabolism in the Caco-2 system results in similar Eadie-Hofstee plots for the receiver side that show nonconformity to simple Michaelis-Menten kinetics (Figs. 9C, 11C, and 13C). The net flux is a consequence of multiple processes involving more than a single barrier, and $C_{D,0}$ cannot estimate the substrate concentration in the vicinity of the transporter or enzyme. The estimated J_{max} is poorly correlated to the true V_{max}, especially for substrates of low diffusive clearance (CL_d < 1 ml/min); the observation persists when

DMD Fast Forward. Published on October 11, 2007 as DOI: 10.1124/dmd.107.015321
This article has not been copyedited and formatted. The final version may differ from this version.

apical influx, secretion or cellular metabolism is the saturable process (Figs. 10, 12 and 14, A-C, Tables 1, 3 and 5). J_{max} is correlated with the true V_{max} only for solutes of high CL_d for apical secretion and absorption but not for cellular metabolism (Figs. 10C, 12C, and 14C). An improved correlation is also observed with reduction of assigned values of V_{max} (< 20 nmol/min) or increased values of $C_{D,0}$ for simulation (data not reported). By contrast, a linear correlation is found between the estimated K'_m or K''_m and K_m when apical influx, secretion or cellular metabolism is the saturable process (Figs. 10, 12, and 14, D-F; Tables 2, 4, and 6). The finding is in contrast to that of Bentz et al. (2005) who commented that a better correlation existed between J_{max} and V_{max} and not K'_m or K''_m and K_m. The correlation is again dependent on values of CL_d, since drugs with higher CL_d equilibrates faster between the donor, cellular, and receiving sites, rendering improvement in the correlation (Figs. 10, 12, and 14 and Table 1-6). K''_m, the parameter obtained by fitting P_c to the Hill-equation-like formula, fails to furnish additional physical meaning or improvement over K'_m in the correlation with K_m. The existence of correlation between effective and true parameters (J_{max} vs. V_{max} and K'_m or K''_m vs. K_m) is useful (Figs. 10, 12,and 14), since changes in J_{max} or K'_m (e.g. induction or inhibition) would commensurate with those of V_{max} or K_m, rendering useful data interpretation on inhibition or induction of transporter or enzyme in the Caco-2 cell system.

For the description of added complexities such as carrier-mediated transport, intracellular metabolism, and saturation of the above processes, we propose use of the catenary model (Fig. 1) for proper data interpretation in the Caco-2 system. The presentation of mass transfer (appendix) in this kinetic model had allowed us to simulate data over time to conduct a thorough theoretical examination on transport and metabolism. Through this exercise, we obtained analytical solutions for EfR under linear conditions, and examined the effects of transport and metabolic intrinsic clearances (CL_{d1}, CL_{d2}, CL_{d3}, CL_{d4}, $CL_{int,sec}$, CL_{abs}, and $CL_{int,met}$). Moreover, the model yielded data on P_c, P_{PD}, and J_c under nonlinear conditions for illustration with the Eadie-Hofstee plots. Although saturation of the basolateral influx or efflux process was not simulated, these patterns could be inferred since the

data would be mirror images of saturable apical influx and efflux. For the first time, trends in EfR according to CL_d and $C_{D,0}$ with varying saturable processes were shown (Fig. 18); EfR values greater than unity would not conclusively reflect involvement of apical efflux transporters since the same trends were observed with saturation in metabolism (Fig. 18C). Although we had not explored a wide parameter space, the analyses showed that the single barrier model for the Caco-2 cell monolayer was inadequate to provide sound estimates of V_{max} and K_m of saturable systems.

The usefulness of the catenary model has been demonstrated fully by the present analysis. In this model, the timed samples collected are utilized fully for data fitting. However, due to the large number of parameters to be ascertained and saturation of one or more of the processes, the fit of the timed-metabolite data may not always lead to fruitful outcomes. A usual strategy is to sum the total amount of formed metabolite (amount in cell + donor + receiver compartments) to describe metabolism in the fitting procedure. Additional data on metabolite transport or metabolic data is absolutely necessary, and would greatly add to the accuracy of the fit (Sun et al., unpublished data). The model was able to describe saturable efflux (Ito et al., 1999), saturable apical absorption and basolateral influx (Irie et al., 2004), and recently, saturable metabolism and substrate inhibition (Sun, et al., unpublished data). Proper data interpretation with the catenary model would definitely remove the bias in parameter estimates, avoid viewing the Caco-2 cell monolayer as a single barrier, and provide accurate estimates.

DMD Fast Forward. Published on October 11, 2007 as DOI: 10.1124/dmd.107.015321
This article has not been copyedited and formatted. The final version may differ from this version.

References

Adachi Y, Suzuki H, and Sugiyama Y (2001) Comparative studies on in vitro methods for evaluating in vivo function of MDR1 P-glycoprotein. *Pharm Res* **18**:1660-1668.

Adson A, Raub TJ, Burton PS, Barsuhn CL, Hilgers AR, Audus KL, and Ho NF (1994) Quantitative approaches to delineate paracellular diffusion in cultured epithelial cell monolayers. *J Pharm Sci* **83**:1529-1536.

Allen JD, van Loevezijn A, Lakhai JM, van der Valk M, van Tellingen O, Reid G, Schellens JH, Koomen GJ, and Schinkel AH (2002) Potent and specific inhibition of the breast cancer resistance protein multidrug transporter in vitro and in mouse intestine by a novel analogue of fumitremorgin C. *Mol Cancer Ther* **1**:417-425.

Bentz J, Tran TT, Polli JW, Ayrton A, and Ellens H (2005) The steady-state Michaelis-Menten analysis of P-glycoprotein mediated transport through a confluent cell monolayer cannot predict the correct Michaelis constant K_m. *Pharm Res* **22**:1667-1677.

Bhardwaj RK, Herrera-Ruiz D, Sinko PJ, Gudmundsson OS, and Knipp G (2005) Delineation of human peptide transporter 1 (hPepT1)- mediated uptake and transport of substrates transfected hPepT1/Madin-Darby canine kidney clones and Caco-2 cells. *J Pharmacol Exp Ther* **314**:1093-1100.

Blais A, Bissonnette P, and Berteloot A (1987) Common characteristics for Na+-dependent sugar transport in Caco-2 cells and human fetal colon. *J Membr Biol* **99**:113-125.

Cummins CL, Mangravite LM, and Benet LZ (2001) Characterizing the expression of CYP3A4 and efflux transporters (P-gp, MRP1, and MRP2) in CYP3A4- transfected caco-2 cells after induction with sodium butyrate and the phorbol ester 12-O- tetradecanoylphorbol-13-acetate. *Pharm Res* **18**:1102-1109.

den Ouden D, van den Heuvel M, Schoester M, van Rens G, and Sonneveld P (1996) In vitro effect of GF120918, a novel reversal agent of multidrug resistance, on acute leukemia and multiple myeloma cells. *Leukemia* **10**:1930-1936.

Fisher JM, Wrighton SA, Watkins PB, Schmiedlin-Ren P, Calamia JC, Shen DD, Kunze KL, Thummel KE (1999) First-pass midazolam metabolism catalyzed by 1α,25-dihydroxy vitamin D3-modified Caco-2 cell monolayers. *J Pharmacol Exp Ther* **289**:1134-1142.

Gekeler V, Ise W, Sanders KH, Ulrich WR, and Beck J (1995) The leukotriene LTD4 receptor antagonist MK571 specifically modulates MRP associated multidrug resistance. *Biochem Biophys Res Commun* **208**:345-352.

González-Alvarez I, Fernández-Teruel C, Garrigues TM, Casabo VG, Ruiz-Garcia A, and Bermejo M (2005) Kinetic modeling of passive transport and active efflux of a fluoroquinolone across Caco-2 cells using a compartmental approach. *Xenobiotica* **35:**1067-1088.

Guo A, Hu P, Balimane PV, Leibach FH, and Sinko PJ (1999) Interactions of a nonpeptidic drug, valacyclovir, with the human intestinal peptide transporter (hPEPT1) expressed in a mammalian cell line. *J Pharmacol Exp Ther* **289**:448-454.

Hidalgo IJ, Raub TJ, and Borchardt RT (1989) Characterization of the human colon carcinoma cell line (Caco-2) as a model system for intestinal epithelial permeability. *Gastroenterology* **96**:736-749.

Hidalgo IJ, Hilgreen KM, Grass GM, and Borchardt RT (1991) Characterization of the unstirred water layer in Caco-2 cell monolayers using a novel diffusion apparatus. *Pharm Res* **8**:222-227.

Hilgers AR, Conradi RA, and Burton PS (1990) Caco-2 cell monolayers as a model for drug transport across the intestinal mucosa. *Pharm Res* **7**:902-910.

Hirohashi T, Suzuki H, Chu XY, Tamai I, Tsuji A, and Sugiyama Y (2000) Function and expression of multidrug resistance-associated protein family in human colon adenocarcinoma cells (Caco-2). *J Pharmacol Exp Ther* **292**:265-270.

Hunter J, Jepson MA, Tsuruo T, Simmons NL, and Hirst BH (1993) Functional expression of P-glycoprotein in apical membranes of human intestinal caco-2 cells. kinetics of vinblastine secretion and interaction with modulators. *J Biol Chem* **268**:14991-14997.

Irie M, Terada T, Okuda M, and Inui K-I (2004) Efflux properties of basolateral peptide transporter in human intestinal cell line Caco-2. *Plugers Arch. Eur J Physiol* **449**:186-194.

Irvine JD, Takahashi L, Lockhart K, Cheong J, Tolan JW, Selick HE, and Grove JR (1999) MDCK (madin-darby canine kidney) cells: A tool for membrane permeability screening. *J Pharm Sci* **88**:28-33.

Ito S, Woodland C, Sarkadi B, Hockmann G, Walker SE, and Koren G (1999) Modeling of P-glycoprotein-involved epithelial drug transport in MDCK cells. *Am J Physiol* **277**:84-96.

Kansy M, Senner F, and Gubernator K (1998) Physicochemical high throughput screening: Parallel artificial membrane permeation assay in the description of passive absorption processes. *J Med Chem* **41**:1007-1010.

Kobayashi D, Nozawa T, Imai K, Nezu J, Tsuji A, Tamai. Involvement of human organic anion transporting polypeptide OATP-B (SLC21A9) in pH-dependent transport across intestinal apical membrane. *J Pharmacol Exp Ther* **306**:703-708.

Lentz KA, Polli JW, Wring SA, Humphreys JE, and Polli JE (2000) Influence of passive permeability on effective P-glycoprotein kinetics. *Pharm Res* **17**:1456-1460.

Okuwaki M, Takada T, Iwayanagi Y, Koh S, Kariya Y, Fujii H, Suzuki H (2007) LXR alpha transactivates mouse organic solute transporter alpha and beta via IR-1 elements shared with FXR. *Pharm Res* **24**:390-398.

Peters WH and Roelofs HM (1989) Time-dependent activity and expression of glutathione S-transferases in the human colon adenocarcinoma cell line caco-2. *Biochem J* **264**:613-616.

Polli JW, Wring SA, Humphreys JE, Huang L, Morgan JB, Webster LO, and Serabjit-Singh CS (2001) Rational use of in vitro P-glycoprotein assays in drug discovery. *J Pharmacol Exp Ther* **299**:620-628.

Stenberg P, Norinder U, Luthman K, Artursson P (2001) Experimental and computational screening methods for the prediction of intestinal drug absorption. *J Med Chem* **44**:1927-1937.

Stephens RH, O'Neill CA, Warhurst A, Carlson GL, Rowland M, Warhurst G (2001) Kinetic profiling of P-glycoprotein-mediated drug efflux in rat and human intestinal epithelia. *J Pharmacol Exp Ther* 296:584-591.

Tam D, Sun H, and Pang KS (2003) Influence of P-glycoprotein, transfer clearances, and drug binding on intestinal metabolism in caco-2 cell monolayers or membrane preparations: A theoretical analysis. *Drug Metab Dispos* **31**:1214-1226.

Tamai I, Saheki A, Saitoh R, Sai Y, Yamada I, and Tsuji A (1997) Nonlinear intestinal absorption of 5-hydroxytryptamine receptor antagonist caused by absorptive and secretory transporters. *J Pharmacol Exp Ther* **283**:108-115.

Thiel-Demby VE, Tippin TK, Humphreys JE, Serabjit-Singh CJ, and Polli JW (2004) In vitro absorption and secretory quotients: Practical criteria derived from a study of 331 compounds to assess for the impact of P-glycoprotein-mediated efflux on drug candidates. *J Pharm Sci* **93**:2567-2572.

Tran TT, Mittal A, Gales T, Maleeff B, Aldinger T, Polli JW, Ayrton A, Ellens H, and Bentz J (2004) Exact kinetic analysis of passive transport across a polarized confluent MDCK cell monolayer modeled as a single barrier. *J Pharm Sci* **93**:2108-2123.

Tran TT, Mittal A, Aldinger T, Polli JW, Ayrton A, Ellens H, and Bentz J (2005) The elementary mass action rate constants of P-gp transport for a confluent monolayer of MDCKII-hMDR1 cells. *Biophys J* **88**:715-738.

Troutman MD and Thakker DR (2003a) Rhoadamine 123 requires carrier-mediated influx for its activity as a P-glycoprotein substrate in Caco-2 cells. *Pharm Res* **20**:1192-1199.

Troutman MD and Thakker DR (2003b) Efflux ratio cannot assess P–glycoprotein- mediated attenuation of absorptive transport: asymmetric effect of P-glycoprotein on absorptive and secretory transport across Caco-2 cell monolayers. *Pharm Res* **20**:1200-1209.

Troutman MD and Thakker DR (2003c) Novel experimental parameters to quantify the modulation of absorptive and secretory transport of compounds by P-glycoprotein in cell culture models of intestinal epithelium. *Pharm Res* **20**:1210-1224.

Usansky HH and Sinko PJ (2005) Estimating human drug oral absorption kinetics from Caco-2 permeability using an absorption-disposition model: model development and evaluation and derivation of analytical solutions for k_a and F_a. *J Pharmacol Exp Ther* **314**:391-399.

Williams GC, Liu A, Knipp G, and Sinko PJ (2002). Direct evidence that saquinavir is transported by mult-drug resistance-associated protein (MRP1) and canalicular multispecific organic anion transporter (MRP2). *Antimicrob Agents Chemother* **46**:3456-3462.

Yamaguchi H, Yano I, Hashimoto Y, and Inui KI (2000) Secretory mechanisms of grepafloxacin and levofloxacin in the human intestinal cell line caco-2. *J Pharmacol Exp Ther* **295**:360-366.

Youdim KA, Avdeef A, Abbott NJ (2003) In vitro trans-monolayer permeability calculations: often forgotten assumptions. *Drug Discov Today* 8:997-1003.

Footnotes

This work was supported by the Canadian Institute for Health Research, grant MOP64350. Send reprint requests to: Dr. K. S. Pang, Faculty of Pharmacy, University of Toronto, 144 College St., Toronto, Ontario, Canada M5S 3M2. E-mail: ks.pang@utoronto.ca

DMD Fast Forward. Published on October 11, 2007 as DOI: 10.1124/dmd.107.015321
This article has not been copyedited and formatted. The final version may differ from this version.

Legends

Figure 1. Schematic presentation of the Caco-2 cell-based system by a catenary model comprising the basolateral (baso), cell, and apical (ap) compartments. V, f, and C denote volume, unbound fraction and the concentration of drugs of each compartment, respectively; M denotes formed metabolite(s). CL_{d1} and CL_{d2}, CL_{d4} and CL_{d3} denote the influx and efflux, passive diffusion clearance on the basolateral and apical membrane, respectively. CL_{influx} and CL_{efflux} represent the transporter-mediated influx and efflux intrinsic clearances on the basolateral membrane; CL_{abs} and $CL_{int,sec}$ denote transporter-mediated intrinsic clearances of absorption and efflux on the apical membrane, respectively; $CL_{int,met}$ is the metabolic intrinsic clearance. Under non-linear conditions, CL_{influx}, CL_{efflux}, CL_{abs} and $CL_{int.sec}$ and $CL_{int,met}$ may be replaced by the $V_{max}/(K_m+C_u)$, where C_u is the unbound drug concentration in cells.

Figure 2. The effective permeability P_{app} according to Eq. 1 for the A→B, and B→A directions, when transporters and enzymes were absent: $CL_{influx} = CL_{efflux} = CL_{int,sec} = CL_{abs} = CL_{int,met} = 0$, and $CL_{d1} = CL_{d2} = CL_{d3} = CL_{d4} = CL_d$. Note, in the insets, P_{app} decreased with cellular binding (f_{cell} denotes the unbound fraction in the cell).

Figure 3. The effective permeability P_{app} vs. time for the A→B and B→A directions when $CL_{d1} = CL_{d2} = CL_{d3} = CL_{d4} = CL_d = 0.2$ ml/min (A) or 0.05 ml/min (B), and the corresponding EfRs, at varying apical efflux activities ($CL_{int,sec}$). All the unbound fractions were equal to unity; $CL_{influx} = CL_{efflux} = CL_{int,met} = CL_{abs} = 0$.

Figure 4. The effective permeability P_{app} vs. time for the A→B, and B→A directions when $CL_{d1} = CL_{d2} = CL_{d3} = CL_{d4} = CL_d = 0.2$ ml/min (A) or 0.05 ml/min (B) at varying cellular metabolic activities ($CL_{int,met}$). All the unbound fractions were equal to unity; $CL_{influx} = CL_{efflux} = CL_{int,sec} = CL_{abs} = 0$.

DMD Fast Forward. Published on October 11, 2007 as DOI: 10.1124/dmd.107.015321
This article has not been copyedited and formatted. The final version may differ from this version.

Figure 5. Influence of $CL_{int,sec}$, together with CL_d (A) and CL_{abs} (B), CL_{influx}/CL_{efflux} (C) on EfR under linear conditions, based on Eq. 12. All passive clearances were assumed to be equal ($CL_{d1} = CL_{d2} = CL_{d3} = CL_{d4} = CL_d$) and unbound fractions in basolateral and apical compartment were equal ($f_{ap} = f_{baso}$). For (A) and (B), $CL_{influx} = CL_{efflux} = 0$ at the basolateral membrane; For (B) and (C), CL_d was assigned as 0.05 ml/min, respectively, and in (A) and (C), $CL_{abs} = 0$.

Figure 6. Influence of Pgp-mediated efflux ($CL_{int,sec}$, from 0 to 5 ml/min) on the asymmetry in metabolite formation at 1 h sampling, expressed as fraction of dose of metabolite formed, f_{met}, from the B→A direction vs. the A→B direction, under linear conditions for solutes of (A) high ($CL_{d1} = CL_{d2} = CL_{d3} = CL_{d4} = CL_d = 0.2$ ml/min) or (B) low ($CL_{d1} = CL_{d2} = CL_{d3} = CL_{d4} = CL_d = 0.05$ ml/min) passive permeability. In all simulations, $CL_{int,met} = 0.05$ ml/min; $CL_{abs} = 0$; $CL_{influx} = CL_{efflux} = 0$ at the basolateral membrane; and unbound fractions were equal to unity.

Figure 7. Effects of saturable, apical efflux ($V_{max} = 50$ nmol/min, $K_m = 10$ μM) on the effect permeability, $P_{app,A\rightarrow B}$, $P_{app,B\rightarrow A}$ and efflux ratio (EfR) for a solute of high (A) and low (B) passive, diffusive clearance ($CL_{d1} = CL_{d2} = CL_{d3} = CL_{d4} = CL_d = 1$ or 0.05 ml/min, respectively). In all simulations, $CL_{abs} = CL_{influx} = CL_{efflux} = 0$, $f_{ap} = f_{baso} = f_{cell} = 1$, $CL_{int,met} = 0.1$ ml/min; $C_{D,0}$ was varied from 0.5 to 500 μM to reach greater degrees of saturation of apical efflux.

Figure 8. Effects of saturable, apical efflux on rates of metabolism, expressed as fraction of dose metabolized ($f_{met,A\rightarrow B}$) and ($f_{met,B\rightarrow A}$), on the asymmetry of metabolism for a solute of high or low passive, diffusive clearance ($CL_{d1} = CL_{d2} = CL_{d3} = CL_{d4} = CL_d = 1$ or 0.05 ml/min, respectively); $CL_{abs} = CL_{influx} = CL_{efflux} = 0$, $f_{ap} = f_{baso} = f_{cell} = 1$, $CL_{int,met} = 0.1$ ml/min. In this simulation, the K_m (10 μM) for apical efflux was kept constant, whereas the V_{max} was varied from 0 to 1,000 nmol/min at $C_{D,0} = 100$ μM.

DMD Fast Forward. Published on October 11, 2007 as DOI: 10.1124/dmd.107.015321
This article has not been copyedited and formatted. The final version may differ from this version.

Figure 9. Effect of saturable, apical efflux (V_{max} = 0.5 nmol/min and K_m = 0.5 μM) on (A) carrier-mediated effective permeability, P_c, (B) the net flux associated with carrier (J_c) at 1 h sampling, and (C) the resulting Eadie-Hofstee plots at different loading concentrations ($C_{D,0}$) in both A→B (open symbols) and B→A (solid symbols) directions, when passive diffusion [CL_d: ○● (0.01 ml/min), ▽▼ (0.1 ml/min), and □■ (1 ml/min) (see inset)] was altered. The unbound fractions were all set to unity; $CL_{int,met}$ was set to 0.01 ml/min; $CL_{influx} = CL_{efflux} = CL_{abs} = 0$. Note the nonconformity of some of the data to Michaelis-Menten kinetics. Usually, the early data points were used to estimate the J_{max} (Y-intercept at $J_c/C_{D,0} = 0$), then the K'_m from the slope ($-K'_m$), or K''_m with an equation associated with the Hill coefficient (Eq. 11).

Figure 10. Correlation between estimated parameter, J_{max} at 1 h sampling, vs. the assigned V_{max} (A, B, and C) and K'_m and K''_m vs. the assigned K_m (D, E, and F) for the apical efflux transporter in the Caco-2 cell monolayer (data of Table 1 and 2), when different CL_d (0.01, 0.1 and 1 ml/min) were used for simulation. In D, E, and F, K'_m (○●) and K''_m (△▲) were represented against K_m. Transport in A→B and B→A directions was denoted by open and solid symbols, respectively. For the simulations, all the unbound fractions were set to unity; $CL_{influx} = CL_{efflux} = CL_{abs} = 0$; $CL_{int,met}$ = 0.01 ml/min.

Figure 11. Effects of saturable, apical absorption (V_{max} = 0.5 nmol/min and K_m = 0.5 μM) on (A) carrier-mediated permeability, P_c, (B) the net flux associated with carrier (J_c) at 1 h sampling, and (C) the resulting Eadie-Hofstee plots at different loading concentrations ($C_{D,0}$) in both A→B (open symbols) and B →A (solid symbols) directions, when passive diffusion [CL_d: ○● (0.01 ml/min), ▽▼ (0.1 ml/min), and □■ (1 ml/min) (see inset)] was altered. The unbound fractions were all set to unity; $CL_{int,met}$ was set to 0.01 ml/min; $CL_{influx} = CL_{efflux} = CL_{int,sec} = 0$. Note the nonconformity of some of the data to Michaelis-Menten kinetics. Usually, the early data points were used to estimate the J_{max}

(Y-intercept at $J_c/C_{D,0} = 0$), then the K'_m from the slope ($-K'_m$), or K''_m with an equation associated with the Hill coefficient (Eq. 11).

Figure 12. Correlation between estimated parameter, J_{max} at 1 h sampling vs. the assigned V_{max} (A, B, and C) and K'_m and K''_m vs. the assigned K_m (D, E, and F) for the absorptive, apical transporter in the Caco-2 cell monolayer (data of Table 3 and 4), when different CL_d (0.01, 0.1 and 1 ml/min) were used for simulation. In (D, E, and F), K'_m (○●) and K''_m (△▲) estimates are plotted against the true K_m. Transport in A→B and B →A directions was denoted by open and solid symbols, respectively. For the simulations, all the unbound fractions were set to unity; $CL_{influx} = CL_{efflux} = CL_{int,sec} = 0$; $CL_{int,met} = 0.01$ ml/min.

Figure 13. Effect of saturable cellular metabolism (V_{max} = 0.5 nmol/min and K_m = 0.5 μM) on (A) carrier-mediated effective permeability, P_c, (B) the net flux associated with carrier (J_c) at 1 h sampling, and (C) the resulting Eadie-Hofstee plots at different loading concentrations ($C_{D,0}$) in both A→B (open symbols) and B→A (solid symbols) directions, when passive diffusion [CL_d: ○● (0.01 ml/min), ▽▼ (0.1 ml/min), and □■ (1 ml/min)] was altered. The unbound fractions were all set to unity; $CL_{influx} = CL_{efflux} = CL_{abs} = CL_{int,sec} = 0$. Note the nonconformity of some of the data to Michaelis-Menten kinetics. Usually, the early data points were used to estimate the J_{max} (Y-intercept at $J_c/C_{D,0} = 0$), then the K'_m from the slope ($-K'_m$), or K''_m with an equation associated with the Hill coefficient (Eq. 11).

Figure 14. Correlation between estimated parameter, J_{max} at 1 h sampling, vs. the assigned V_{max} (A, B,and C) and K'_m and K''_m vs. the assigned K_m (D, E, and F) for saturable cellular metabolic activity in the Caco-2 cell monolayer (data of Table 5 and 6), when different CL_d (0.01, 0.1 and 1 ml/min) were used for simulation. Transport in A→B and B→A directions was denoted by open and solid symbols, respectively. In (B), K'_m and K''_m

were represented by ○● and △▲, respectively. For the simulations, all the unbound fractions were set to unity; $CL_{influx} = CL_{efflux} = CL_{abs} = CL_{int,sec} = 0$.

Figure 15. Time and concentration dependent profiles of J_c in A→B (upper panel) and B →A (lower panel) directions, when saturation of (A) apical efflux (V_{max} = 0.5 nmol/min, K_m = 0.5 μM; $CL_{influx} = CL_{efflux} = CL_{abs} = CL_{int,met} = 0$), (B) apical absorption (V_{max} = 0.5 nmol/min, K_m = 0.5 μM; $CL_{influx} = CL_{efflux} = CL_{int,sec} = CL_{int,met} = 0$) and (C) metabolism ($V_{max}$ = 0.5 nmol/min, K_m = 0.5 μM, and $CL_{influx} = CL_{efflux} = CL_{int,sec} = CL_{abs} = 0$) were examined. The simulations were set as follows: $CL_{d1} = CL_{d2} = CL_{d3} = CL_{d4} = CL_d$ = 0.1 ml/min; the unbound fractions were set to unity.

Figure 16. Modulation of metabolite formation ($CL_{int,met}$ = 0.01 ml/min) by saturable efflux (A, E) or influx (B, F) on the apical membrane, or efflux (C, G) or influx (D, H) on the basolateral membrane, for drugs of high CL_d ($CL_d = CL_{d1} = CL_{d2} = CL_{d3} = CL_{d4}$ = 1 ml/min) (A to D) or low CL_d (0.01 ml/min) (E to H). Simulation was performed at $C_{D,0}$ = 100 μM when only one saturable pathway existed (K_m =0.5 μM and V_{max} was varied from 0.5 to 50 nmol/min); all the unbound fractions were set to be unity.

Figure 17. Modulation of metabolite formation by saturable efflux (A,E) or influx (B,F) on the apical membrane, or efflux (C,G) or influx (D,H) on the basolateral membrane for drugs of high CL_d ($CL_d = CL_{d1} = CL_{d2} = CL_{d3} = CL_{d4}$ = 1 ml/min) (A to D) or low CL_d (0.01 ml/min) (E to H). Simulation was performed for $C_{D,0}$ = 1 to 500 μM, with sampling at 1 h, when only one saturable pathway of K_m = 0.5 μM and V_{max} was varied from 0.5 to 50 nmol/min existed; $CL_{int,met}$ = 0.01 ml/min and all the unbound fractions were set to be unity.

Figure 18. Modulation of the efflux ratio (EfR), estimated at 1 h for sampling, by saturable apical efflux (A), apical influx (B) and intracellular metabolism (C). The value of EfR = 1 was denoted by ------. In (A) and (B), $CL_{int,met}$ = 0.01ml/min. Only one saturable component

DMD Fast Forward. Published on October 11, 2007 as DOI: 10.1124/dmd.107.015321
This article has not been copyedited and formatted. The final version may differ from this version.

(V_{max} = 0.5 nmol/min and K_m = 0.5 μM) was present at a time. For simulation, the following assumptions were made: CL_d = CL_{d1} = CL_{d2} = CL_{d3} = CL_{d4} = 0.01, 0.1 or 1 ml/min; all the unbound fractions equaled unity.

Table 1. Correlation between V_{max} and J_{max}, for apical efflux at various CL_d, when $CL_{int,met}$ = 0.01 ml/min and K_m = 0.5 μM; CL_{influx} = CL_{efflux} = CL_{abs} = 0 and CL_{d1} = CL_{d2} = CL_{d3} = CL_{d4} = CL_d; all the unbound fractions are set to be unity.

Assigned V_{max} (nmol/min)	**A → B**				**B → A**			
	J_{max} (nmol/min)	K'_m* (μM)	K''_m* (μM)	β	J_{max} (nmol/min)	K'_m* (μM)	K''_m* (μM)	β
Case 1 (CL_d = 0.01 ml/min)								
0.05	0.0134	1.75	3.75	1.20	0.0288	1.62	3.45	1.20
0.5	0.134	2.49	17.4	1.62	0.288	2.23	16.2	1.63
5	14.9	5.40×10^3	5.34×10^3	1.01	17.4	2.62×10^3	2.58×10^3	1.01
25	7.45×10^3	2.78×10^6	2.78×10^6	1.00	1.56×10^4	2.52×10^6	2.52×10^6	1.00
50	3.50×10^4	1.30×10^7	1.30×10^7	1.00	7.44×10^4	1.20×10^7	1.20×10^7	1.00
Case 2 (CL_d = 0.1 ml/min)								
0.05	0.00641	1.66	1.71	1.01	0.00824	0.867	1.09	1.04
0.5	0.0640	1.60	3.57	1.21	0.0825	0.967	2.19	1.20
5	0.641	2.26	17.1	1.64	0.825	1.22	11.5	1.69
25	3.90	113	161	1.18	4.18	8.34	49.7	1.53
50	74.7	5.66×10^3	5.60×10^3	1.01	14.4	379	407	1.08
Case 3 (CL_d = 1 ml/min)								
0.05	0.000671	1.58	1.59	1.00	0.000848	0.922	0.938	1.00
0.5	0.00671	1.58	1.77	1.03	0.00848	0.930	1.03	1.02
5	0.0671	1.63	3.63	1.21	0.0848	0.946	2.05	1.19
25	0.336	1.89	10.6	1.53	0.424	1.03	6.43	1.53
50	0.672	2.32	17.2	1.63	0.849	1.16	10.8	1.68

* the true K_m is 0.5 μM

Table 2. Correlation between K_m, K'_m and K''_m for apical efflux at various CL_d, when $CL_{int,met}$ = 0.01 ml/min and V_{max} = 0.5 nmol/min; $CL_{influx} = CL_{efflux} = CL_{abs} = 0$ and $CL_{d1} = CL_{d2} = CL_{d3} = CL_{d4} = CL_d$; all the unbound fractions are set to be unity.

Assigned K_m (μM)	**A → B**				**B → A**			
	J_{max}* (nmol/min)	K'_m (μM)	K''_m (μM)	β	J_{max}* (nmol/min)	K'_m (μM)	K''_m (μM)	β
Case 1 (CL_d = 0.01 ml/min)								
0.05	0.134	0.252	12.0	2.10	0.288	0.226	11.2	2.12
0.5	0.134	2.49	17.4	1.62	0.288	2.23	16.2	1.63
5	0.135	23.9	39.0	1.20	0.290	21.5	36.0	1.21
25	0.138	109	116	1.04	0.296	99.3	107	1.05
50	0.139	205	209	1.02	0.298	188	192	1.02
Case 2 (CL_d = 0.1 ml/min)								
0.05	0.0640	0.173	1.49	1.49	0.0825	0.0874	0.857	1.46
0.5	0.0640	1.60	3.57	1.21	0.0825	0.967	2.19	1.20
5	0.0640	15.8	17.7	1.04	0.0825	9.78	11.2	1.05
25	0.0640	78.6	79.4	1.01	0.0826	48.8	49.6	1.01
50	0.0640	156	156	1.00	0.0826	97.4	97.9	1.00
Case 3 (CL_d = 1 ml/min)								
0.05	0.00671	0.160	0.233	1.06	0.00848	0.0908	0.123	1.04
0.5	0.00671	1.58	1.78	1.03	0.00848	0.930	1.03	1.02
5	0.00671	15.8	16.0	1.01	0.00848	9.22	9.40	1.01
25	0.00672	79.4	79.3	1.00	0.00849	46.4	46.5	1.00
50	0.00671	158	158	1.00	0.00849	92.8	92.8	1.00

* the true V_{max} = 0.5 nmol/min

Table 3. Correlation between V_{max} and J_{max}, for apical influx at various CL_d, when $CL_{int,met}$ = 0.01 ml/min and K_m = 0.5 μM; CL_{influx} = CL_{efflux} = $CL_{int,sec}$ = 0 and CL_{d1} = CL_{d2} = CL_{d3} = CL_{d4} = CL_d; all the unbound fractions are set to be unity.

Assigned V_{max} (nmol/min)	**A → B**				**B → A**			
	J_{max} (nmol/min)	K'_m * (μM)	K''_m* (μM)	β	J_{max} (nmol/min)	K'_m * (μM)	K''_m* (μM)	β
Case 1 (CL_d = 0.01 ml/min)								
0.05	0.0134	0.581	0.864	1.08	0.0285	14.8	14.6	1.01
0.5	0.134	0.612	5.28	1.62	0.289	25.3	51.1	1.29
5	1.34	1.38	34.1	1.82	331	1.24×10^5	1.24×10^5	1.00
25	-86.4	-1.02×10^4	NA	NA	1.60×10^4	5.99×10^6	5.99×10^6	1.00
50	-157	-1.87×10^4	NA	NA	6.86×10^4	2.56×10^7	2.56×10^7	1.00
Case 2 (CL_d = 0.1 ml/min)								
0.05	0.00640	1.15	1.66	1.08	0.00825	1.40	1.28	0.99
0.5	0.0640	1.34	5.22	1.39	0.0825	1.35	3.51	1.26
5	0.642	2.66	28.7	1.73	0.826	2.01	19.4	1.70
25	-38.3	-6608	NA	NA	6.91	343	374	1.08
50	-28.8	-5229	NA	NA	1199	9.36×10^4	9.35×10^4	1.00
Case 3 (CL_d = 1 ml/min)								
0.05	0.000671	1.60	1.61	1.00	0.000848	0.91	0.95	1.01
0.5	0.00671	1.59	2.02	1.06	0.00848	0.93	1.15	1.04
5	0.0671	1.70	5.95	1.36	0.0848	0.97	3.33	1.32
25	0.336	2.39	18.3	1.65	0.424	1.18	11.1	1.69
50	0.674	4.18	32.7	1.61	0.849	1.54	18.5	1.75

* the true K_m is 0.5 μM

Table 4. Corelation between K_m (0.5 μM), K'_m and K''_m for apical influx at various CL_d, when $CL_{int,met}$ = 0.01 ml/min and V_{max} = 0.5 nmol/min; CL_{influx} = CL_{efflux} = $CL_{int,sec}$ = 0 and CL_{d1} = CL_{d2} = CL_{d3} = CL_{d4} = CL_d; all the unbound fractions are set to be unity.

Assigned K_m (μM)	**A → B**				**B → A**			
	J_{max}* (nmol/min)	K'_m (μM)	K''_m (μM)	β	J_{max}* (nmol/min)	K'_m (μM)	K''_m (μM)	β
Case 1 (CL_d = 0.01 ml/min)								
0.05	0.134	0.0613	3.96	2.10	0.288	4.70	31.6	1.60
0.5	0.134	0.612	5.28	1.62	0.289	25.3	51.1	1.29
5	0.134	6.11	10.3	1.18	0.284	133	140	1.04
25	0.134	30.4	33.0	1.04	0.264	450	450	1.00
50	0.134	60.3	62.1	1.02	0.253	799	799	1.00
Case 2 (CL_d = 0.1 ml/min)								
0.05	0.0640	0.100	3.04	1.85	0.0825	0.180	1.78	1.55
0.5	0.0640	1.34	5.22	1.39	0.0825	1.35	3.50	1.26
5	0.0641	13.7	17.4	1.09	0.0824	12.0	13.8	1.05
25	0.0642	67.4	69.2	1.02	0.0822	56.6	57.2	1.01
50	0.0643	133	134	1.00	0.0820	110	111	1.00
Case 3 (CL_d = 1 ml/min)								
0.05	0.00671	0.161	0.378	1.15	0.00848	0.0919	0.172	1.10
0.5	0.00671	1.58	2.02	1.06	0.00848	0.934	1.14	1.04
5	0.00671	15.8	16.3	1.01	0.00848	9.32	9.57	1.01
25	0.00671	79.1	79.4	1.00	0.00849	46.5	46.6	1.00
50	0.00672	158	158	1.00	0.00848	92.8	92.9	1.00

* the true V_{max} = 0.5 nmol/min

Table 5. Correlation between V_{max} and J_{max}, for cellular metabolism (K_m = 0.5 μM) at various CL_d when other satiable components (apical/basolateral influx, efflux) are absent: $CL_{influx} = CL_{efflux} = CL_{int,sec} = CL_{abs} = 0$ and $CL_{d1} = CL_{d2} = CL_{d3} = CL_{d4} = CL_d$; all the unbound fractions are set to be unity.

Assigned V_{max} (nmol/min)	**A → B**				**B → A**			
	J_{max} (nmol/min)	K'_m * (μM)	K''_m* (μM)	β	J_{max} (nmol/min)	K'_m * (μM)	K''_m* (μM)	β
Case 1 (CL_d = 0.01 ml/min)								
0.05	0.0256	1.13	3.40	1.29	0.0238	1.05	3.13	1.28
0.5	0.256	1.75	18.4	1.72	0.238	1.57	17.1	1.73
5	124	2.92×10^4	2.91×10^4	1.00	92.4	2.17×10^4	2.16×10^4	1.00
25	2.81×10^4	6.82×10^6	6.82×10^6	1.00	2.65×10^4	6.27×10^6	6.27×10^6	1.00
50	1.32×10^5	3.11×10^7	3.11×10^7	1.00	1.22×10^5	2.89×10^7	2.89×10^7	1.00
Case 2 (CL_d = 0.1 ml/min)								
0.05	0.0293	1.23	1.87	1.10	0.0205	0.858	1.26	1.08
0.5	0.293	1.37	8.20	1.53	0.205	0.927	5.59	1.51
5	3.21	50.1	96.3	1.26	2.06	2.79	35.6	1.69
25	199	1.32×10^4	1.31×10^4	1.00	267	1.77×10^4	1.76×10^4	1.00
50	1.09×10^4	7.27×10^5	7.27×10^5	1.00	2.20×10^4	1.48×10^6	1.48×10^6	1.00
Case 3 (CL_d = 1 ml/min)								
0.05	0.0310	1.34	1.80	1.07	0.0189	0.812	1.05	1.05
0.5	0.310	1.43	7.63	1.51	0.189	0.846	4.52	1.47
5	3.15	10.0	57.8	1.52	1.89	1.51	29.2	1.79
25	1.34×10^7	8.60×10^8	8.60×10^8	1.00	1.08×10^5	6.93×10^6	6.93×10^6	1.00
50	3.41×10^9	2.19×10^{11}	2.19×10^{11}	1.00	4.11×10^9	2.64×10^{11}	2.64×10^{11}	1.00

* the true K_m is 0.5 μM

Table 6. Correlation between K_m, K'_m and K''_m for cellular metabolism at various CL_d, when when other satiable components (apical/basolateral influx, efflux) are absent: $CL_{influx} = CL_{efflux} = CL_{int,sec} = CL_{abs} = 0$ and $CL_{d1} = CL_{d2} = CL_{d3} = CL_{d4} = CL_d$; all the unbound fractions are set to be unity.

Assigned K_m (μM)	**A → B**				**B → A**			
	J_{max}* (nmol/min)	K'_m (μM)	K''_m (μM)	β	J_{max}* (nmol/min)	K'_m (μM)	K''_m (μM)	β
Case 1 (CL_d = 0.01 ml/min)								
0.05	0.256	0.179	13.4	2.19	0.238	0.160	12.6	2.20
0.5	0.256	1.75	18.4	1.72	0.238	1.57	17.1	1.73
5	0.258	16.7	35.2	1.29	0.240	15.0	32.6	1.29
25	0.263	75.9	87.7	1.08	0.244	69.2	80.8	1.08
50	0.266	142	149	1.04	0.247	130	137	1.04
Case 2 (CL_d = 0.1 ml/min)								
0.05	0.293	0.139	6.02	2.03	0.205	0.0951	3.93	1.98
0.5	0.293	1.37	8.20	1.53	0.205	0.927	5.59	1.51
5	0.293	13.6	20.0	1.14	0.206	9.21	13.9	1.15
25	0.295	66.7	70.0	1.03	0.206	45.6	48.6	1.03
50	0.295	131	133	1.01	0.207	90.3	92.1	1.01
Case 3 (CL_d = 1 ml/min)								
0.05	0.310	0.143	5.40	2.00	0.189	0.0847	3.34	1.94
0.5	0.310	1.43	7.63	1.51	0.189	0.846	4.52	1.47
5	0.310	14.3	19.1	1.11	0.189	8.45	11.6	1.11
25	0.311	70.4	72.7	1.02	0.189	42.0	43.9	1.02
50	0.312	139	140	1.01	0.190	83.6	84.8	1.01

* the true V_{max} = 0.5 nmol/min

Figure 1

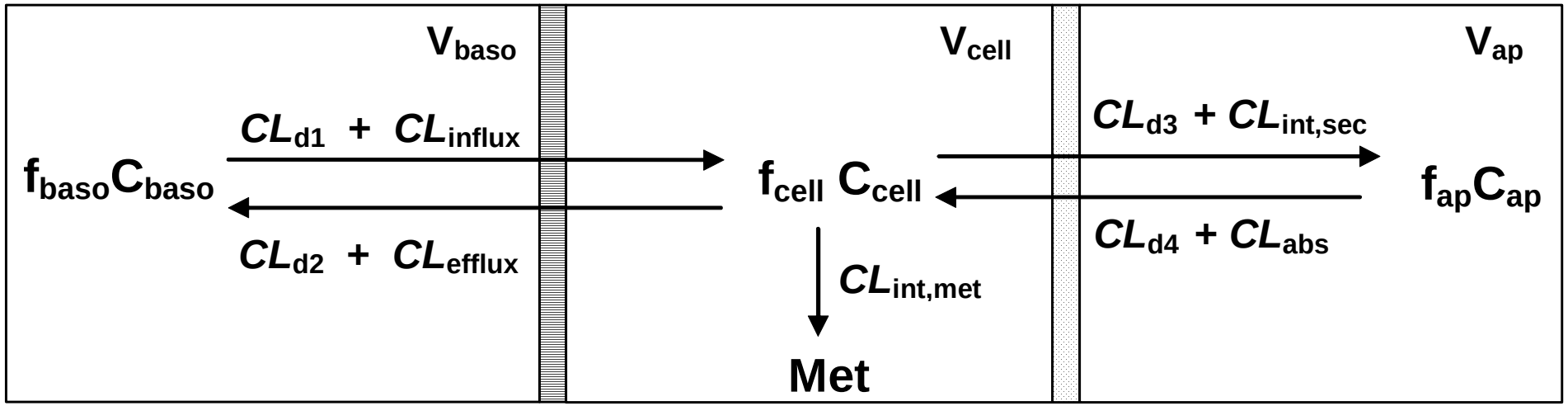

DMD Fast Forward. Published on October 11, 2007 as DOI: 10.1124/dmd.107.015321
This article has not been copyedited and formatted. The final version may differ from this version.

Figure 2

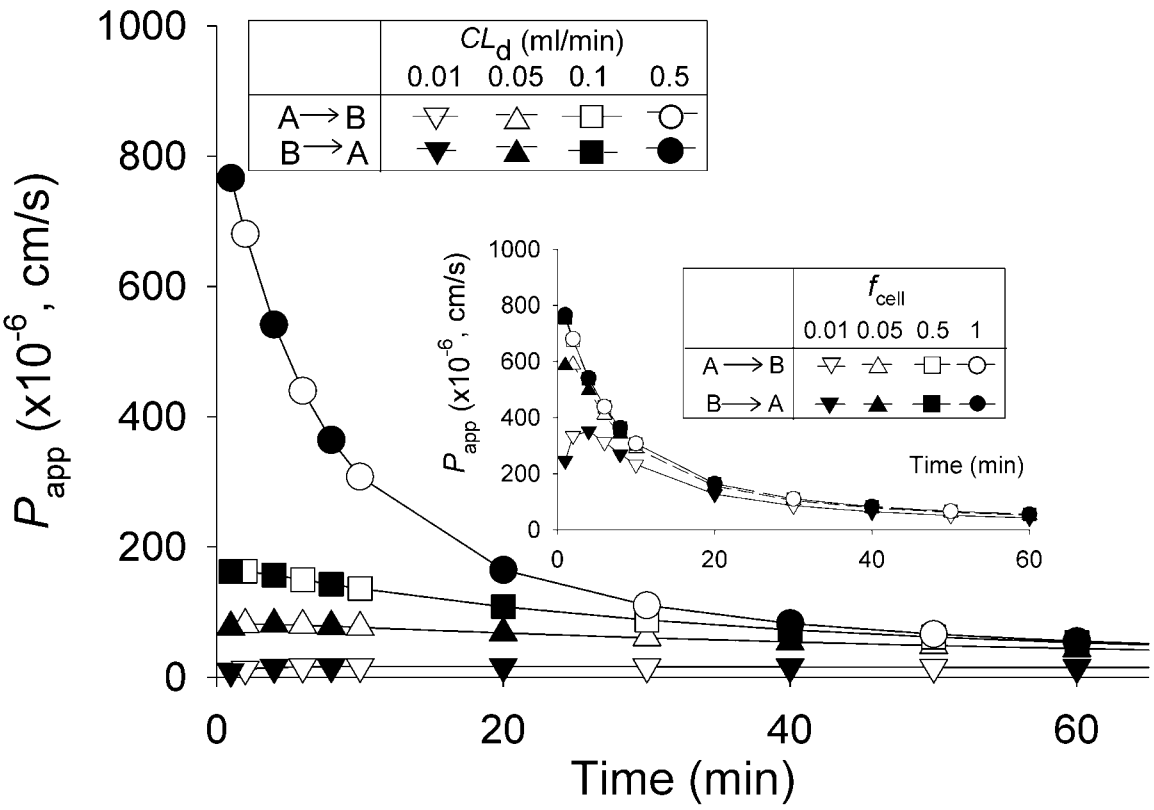

Figure 3

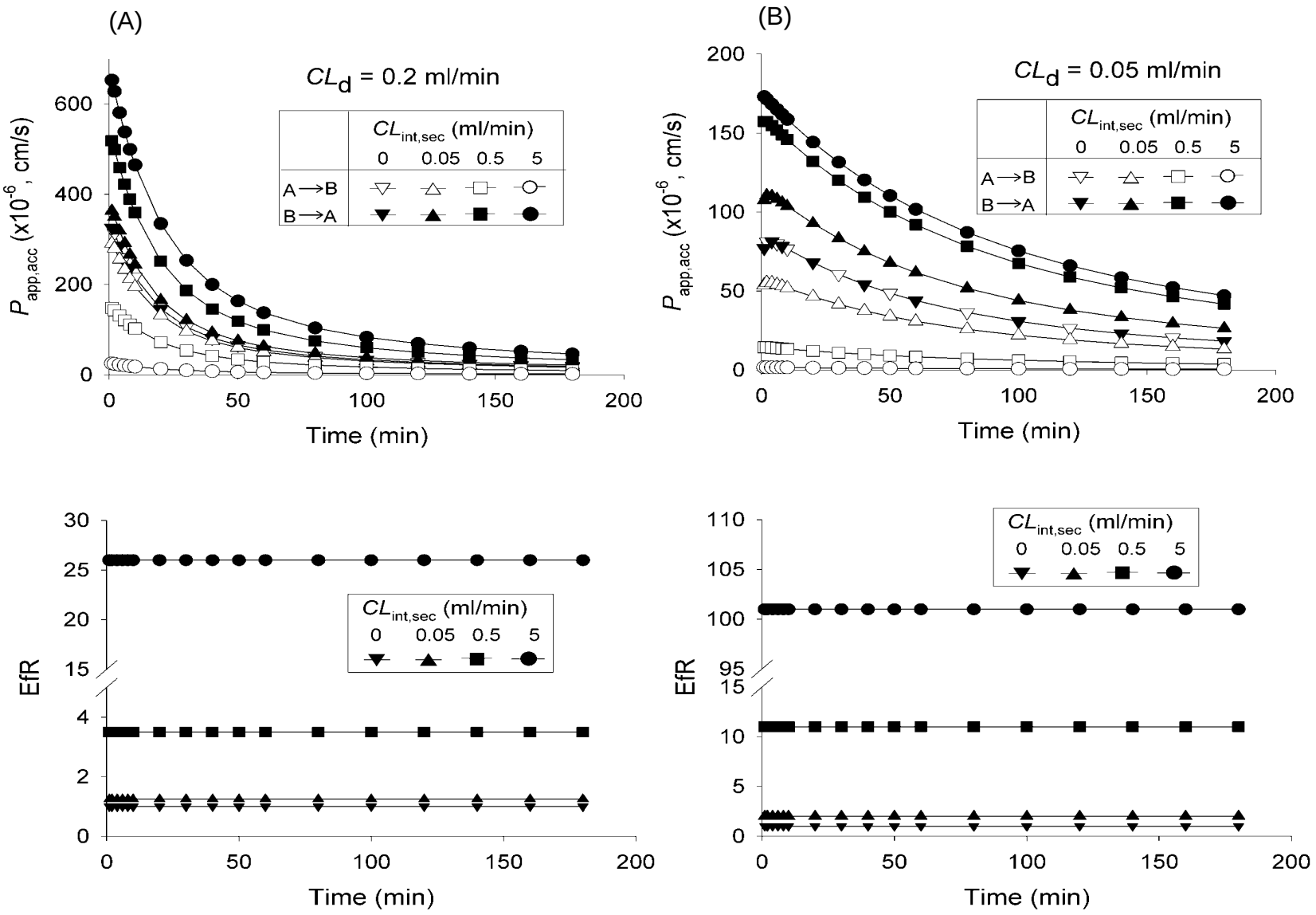

Figure 4

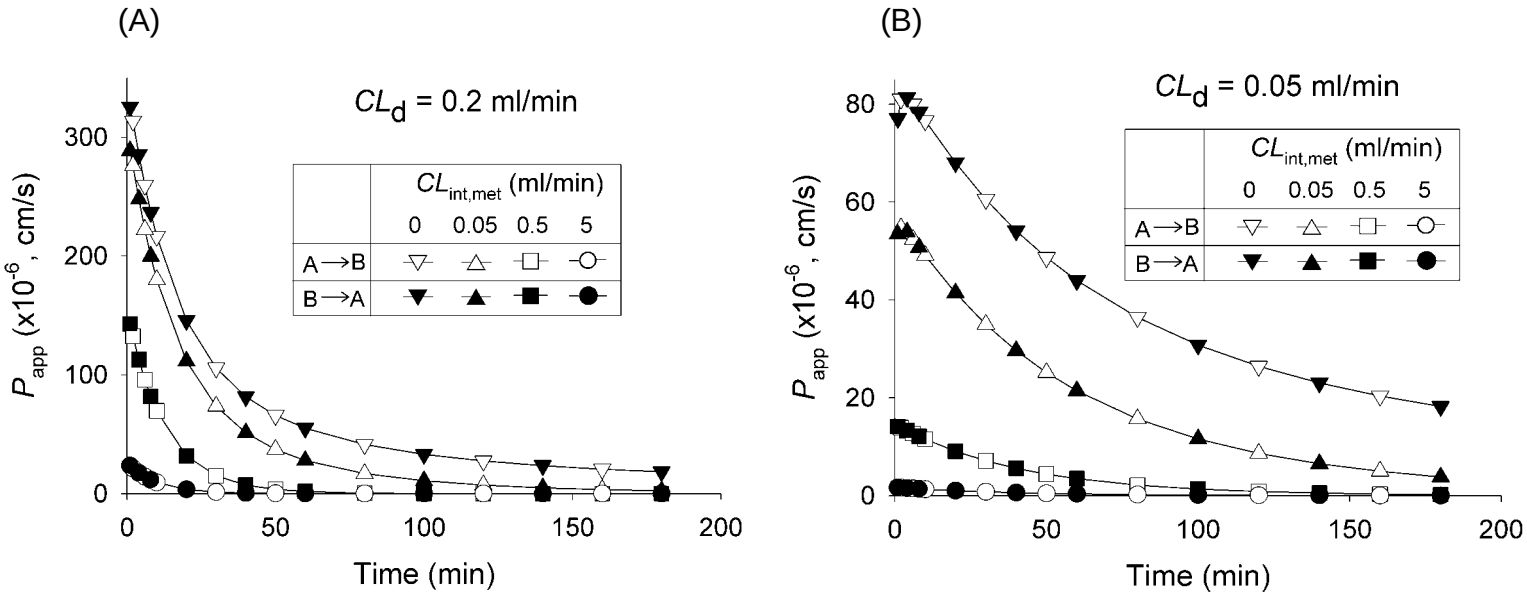

Figure 5

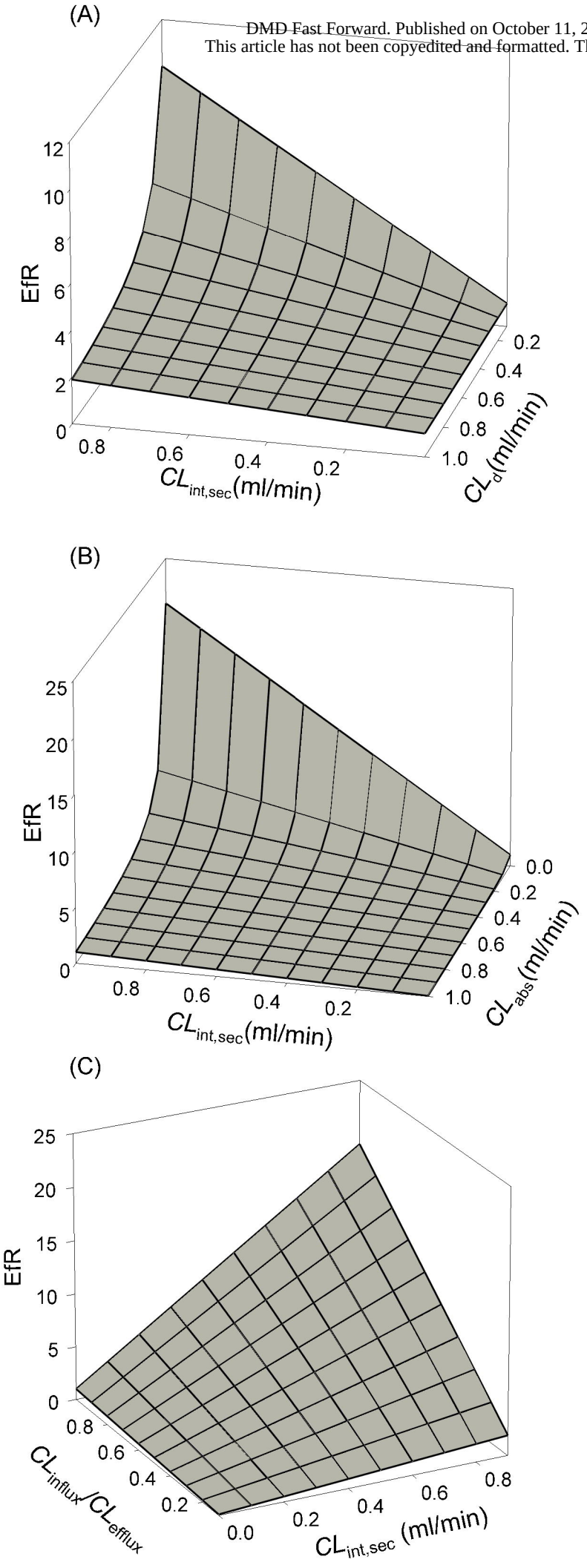

DMD Fast Forward. Published on October 11, 2007 as DOI: 10.1124/dmd.107.015321
This article has not been copyedited and formatted. The final version may differ from this version.

Figure 6

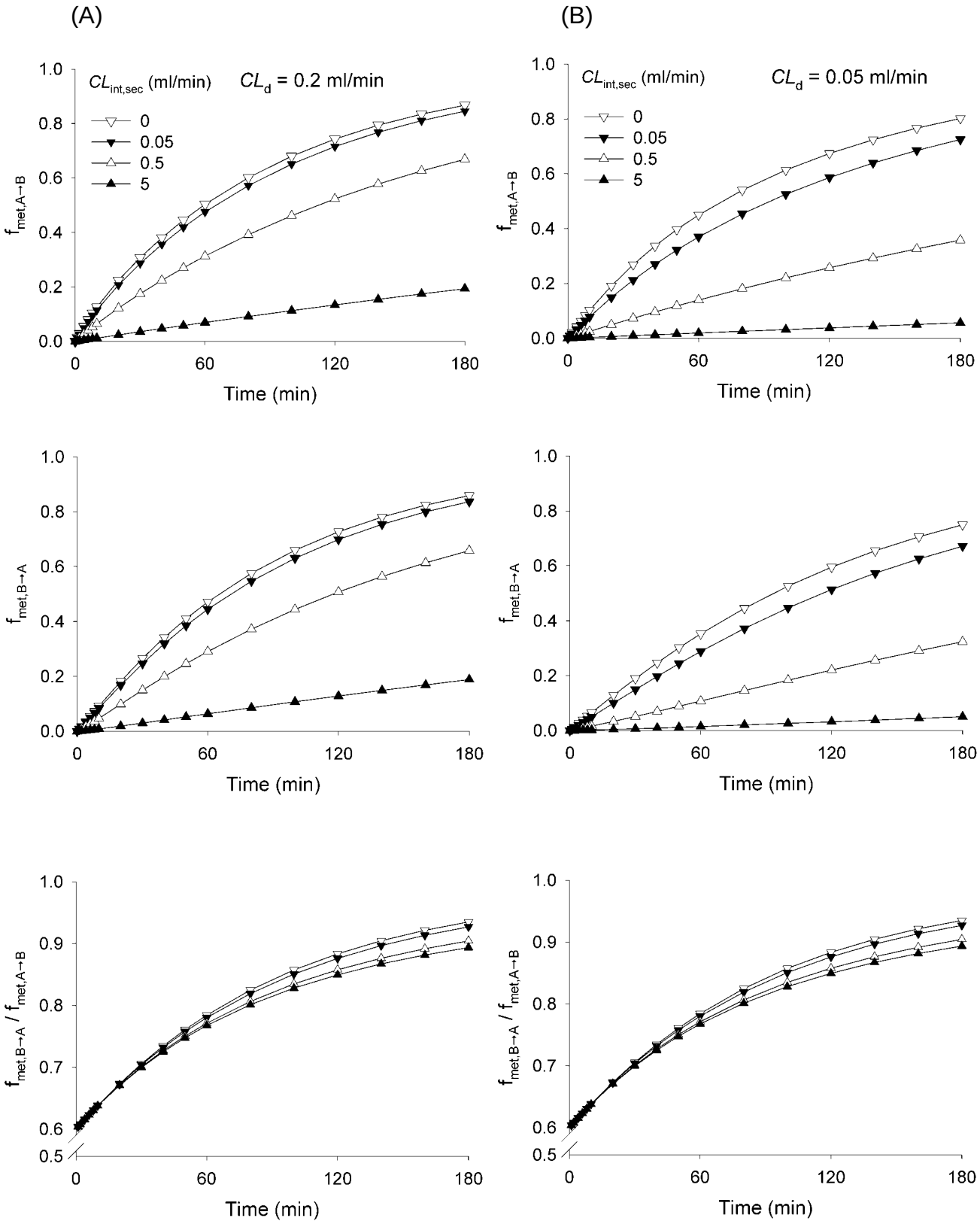

DMD Fast Forward. Published on October 11, 2007 as DOI: 10.1124/dmd.107.015321
This article has not been copyedited and formatted. The final version may differ from this version.

Figure 7

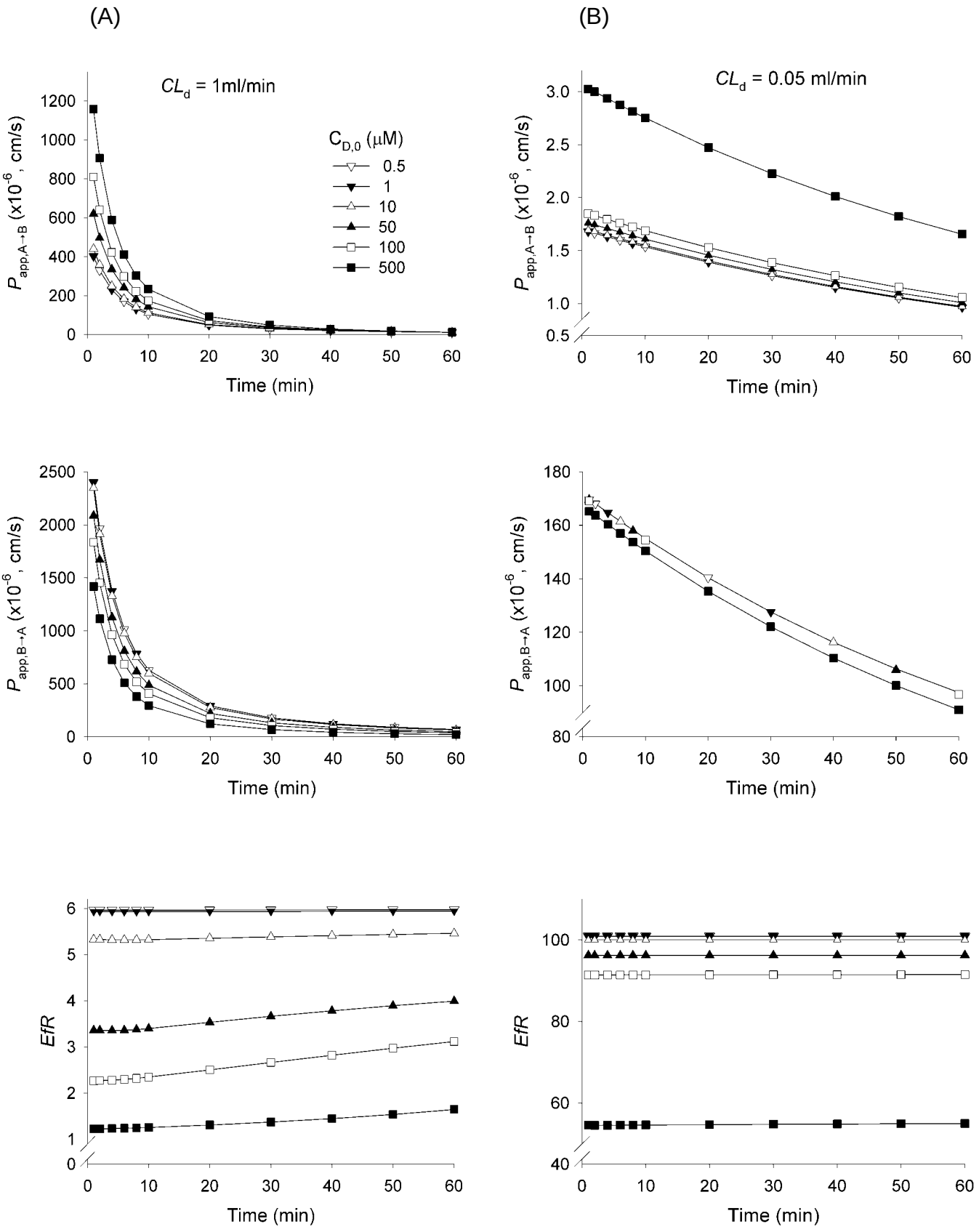

DMD Fast Forward. Published on October 11, 2007 as DOI: 10.1124/dmd.107.015321
This article has not been copyedited and formatted. The final version may differ from this version.

Figure 8

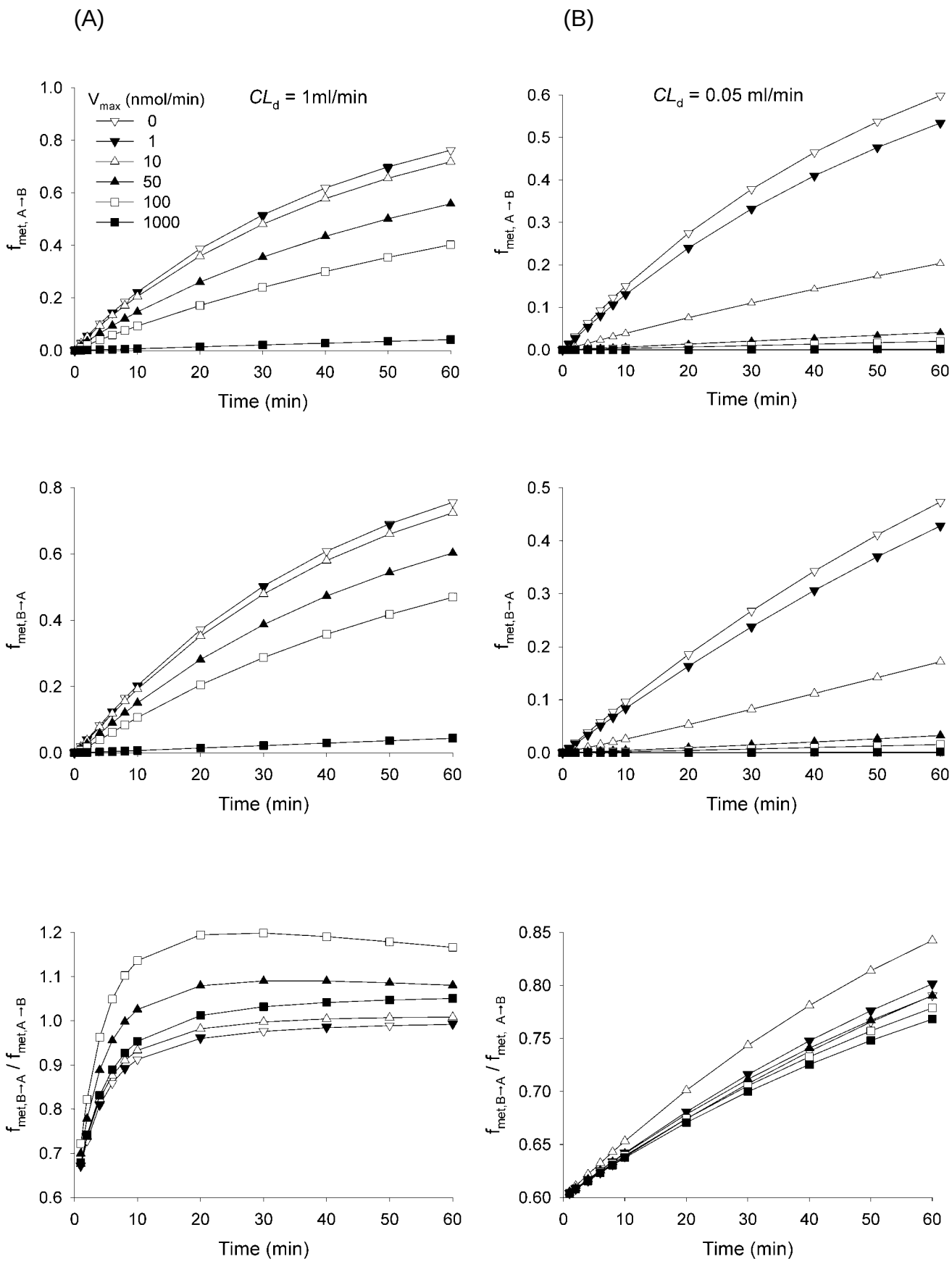

DMD Fast Forward. Published on October 11, 2007 as DOI: 10.1124/dmd.107.015321
This article has not been copyedited and formatted. The final version may differ from this version.

Figure 9

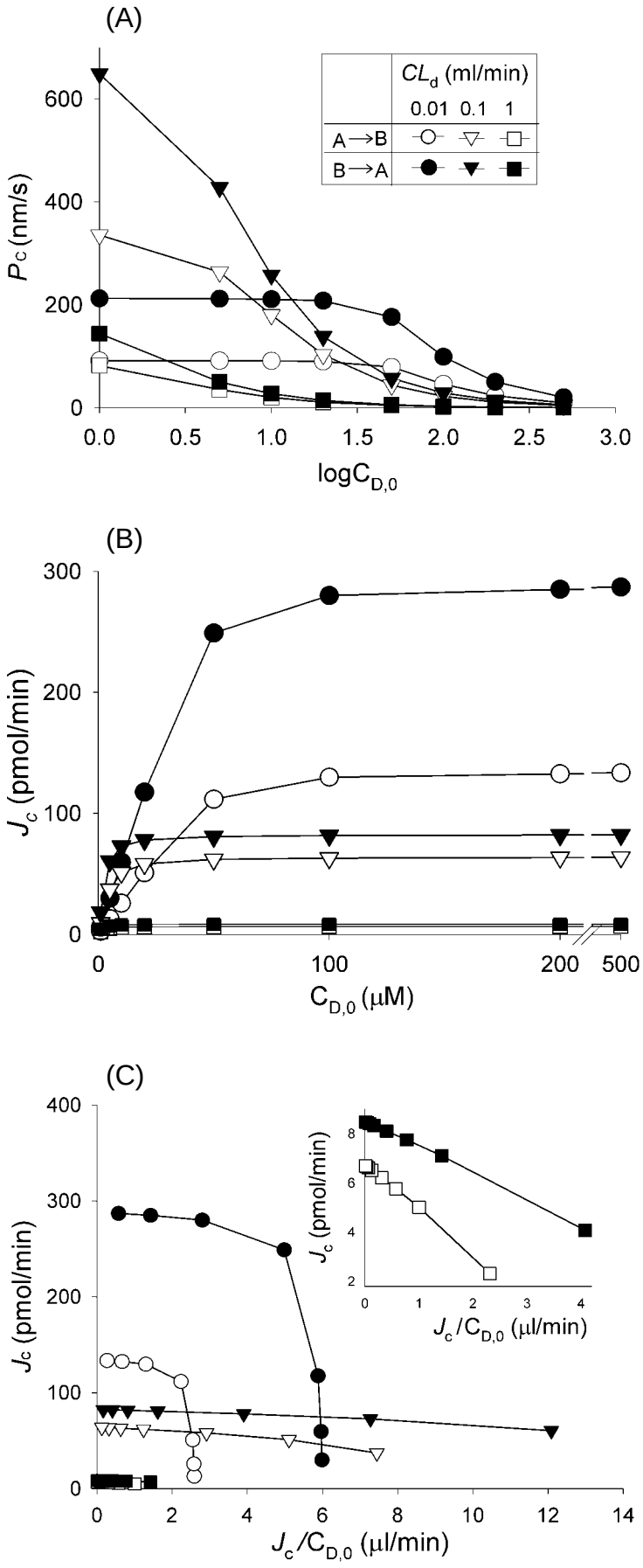

DMD Fast Forward. Published on October 11, 2007 as DOI: 10.1124/dmd.107.015321
This article has not been copyedited and formatted. The final version may differ from this version.

Figure 10

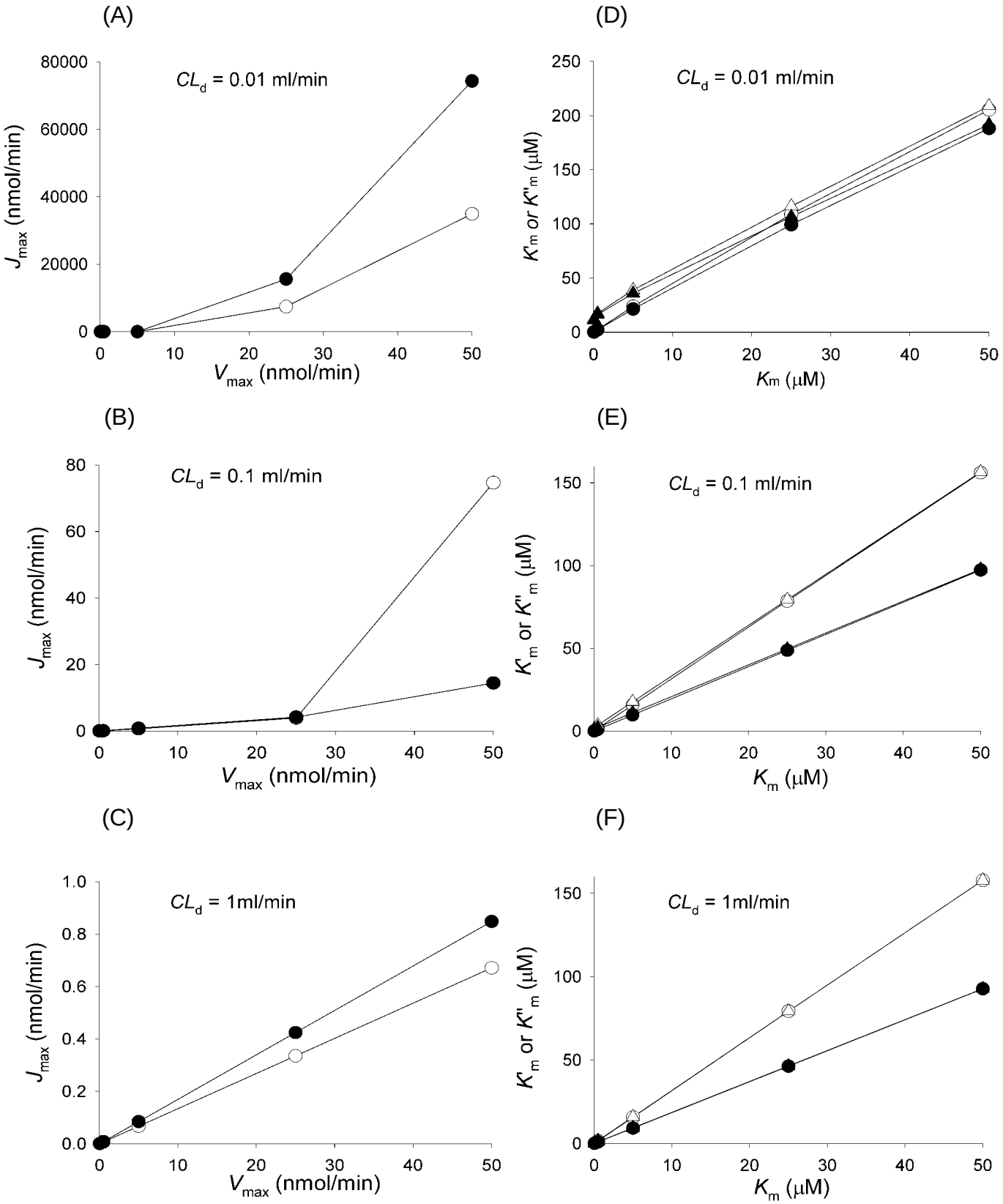

DMD Fast Forward. Published on October 11, 2007 as DOI: 10.1124/dmd.107.015321
This article has not been copyedited and formatted. The final version may differ from this version.

Figure 11

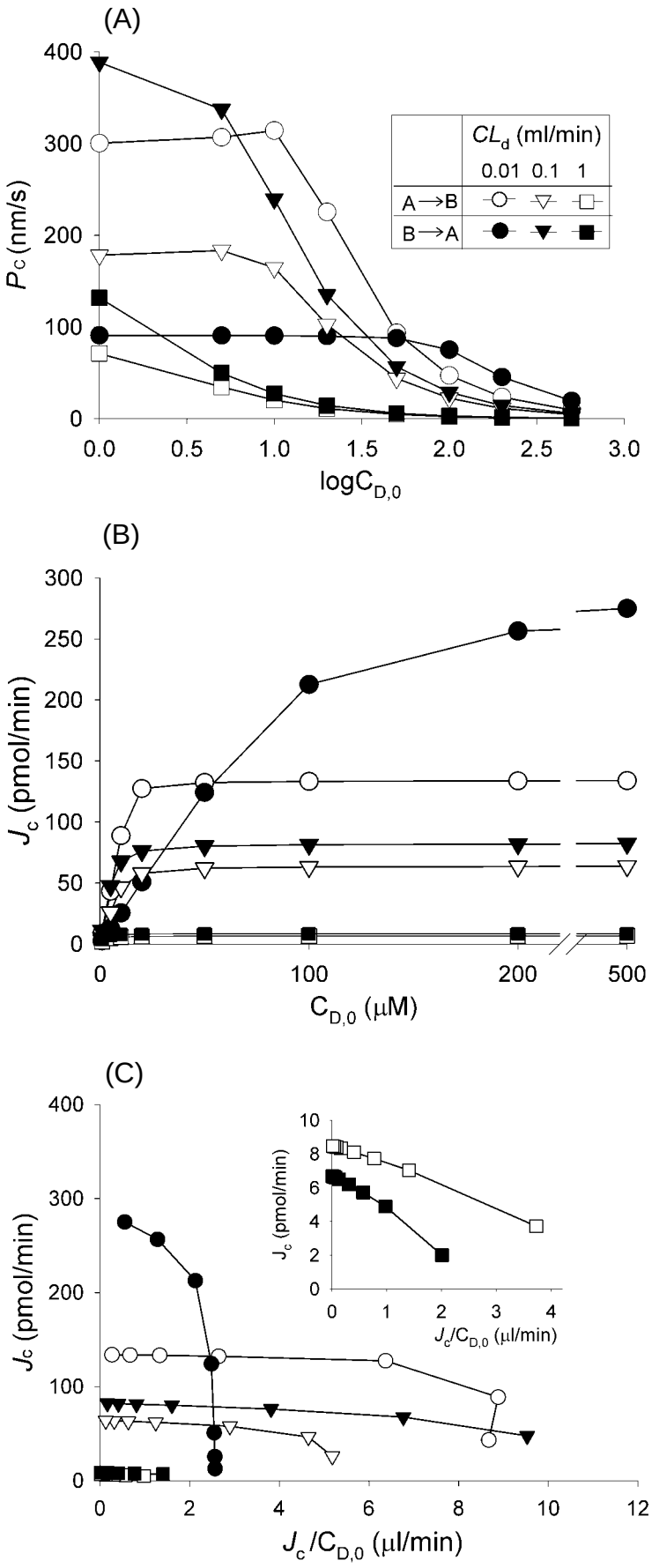

DMD Fast Forward. Published on October 11, 2007 as DOI: 10.1124/dmd.107.015321
This article has not been copyedited and formatted. The final version may differ from this version.

Figure 12

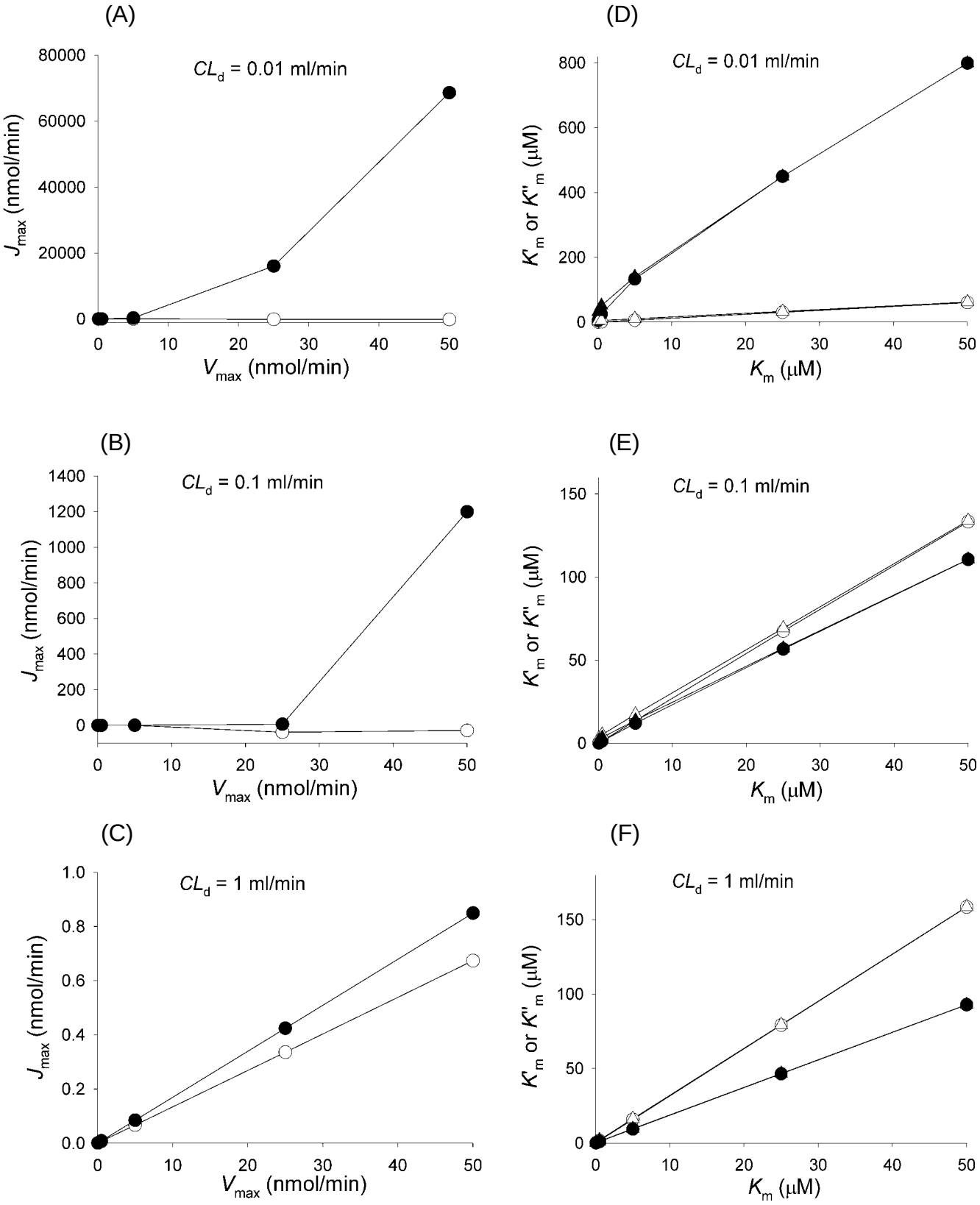

DMD Fast Forward. Published on October 11, 2007 as DOI: 10.1124/dmd.107.015321
This article has not been copyedited and formatted. The final version may differ from this version.

Figure 13

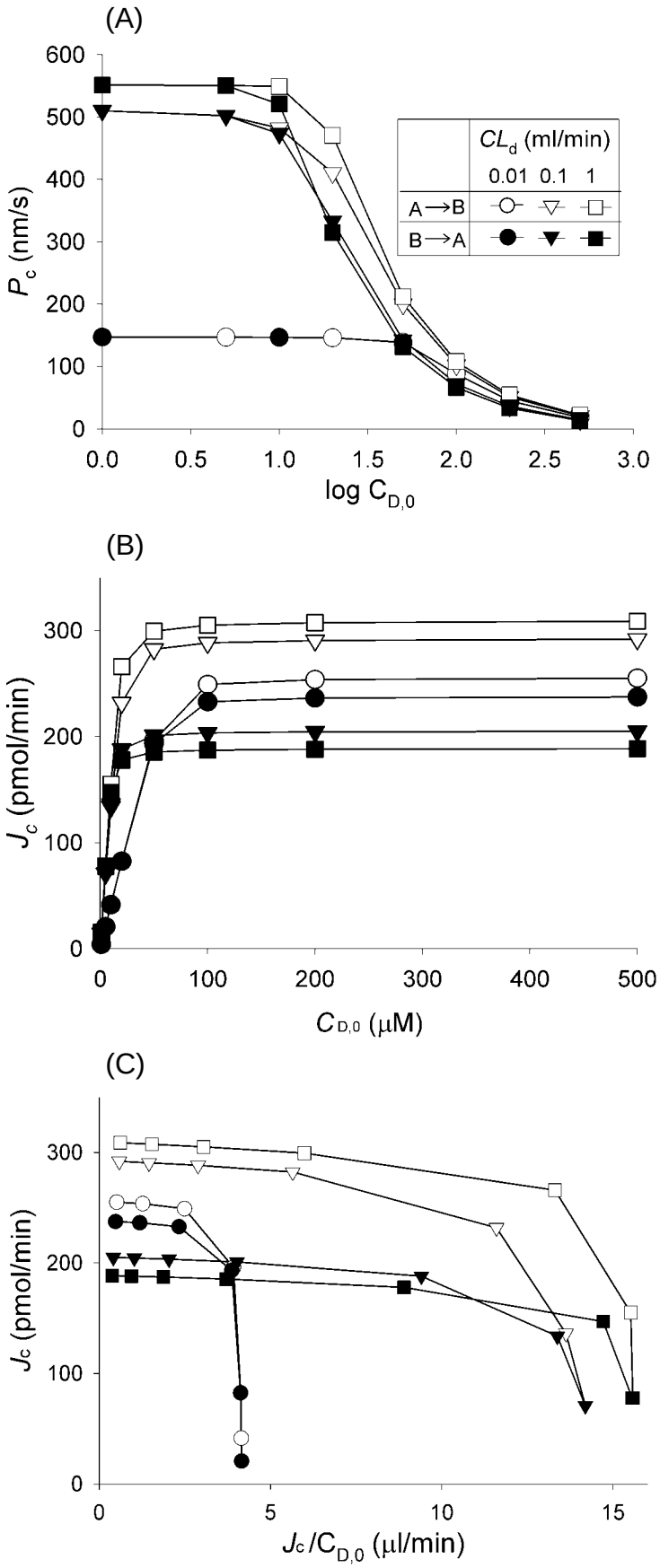

DMD Fast Forward. Published on October 11, 2007 as DOI: 10.1124/dmd.107.015321
This article has not been copyedited and formatted. The final version may differ from this version.

Figure 14

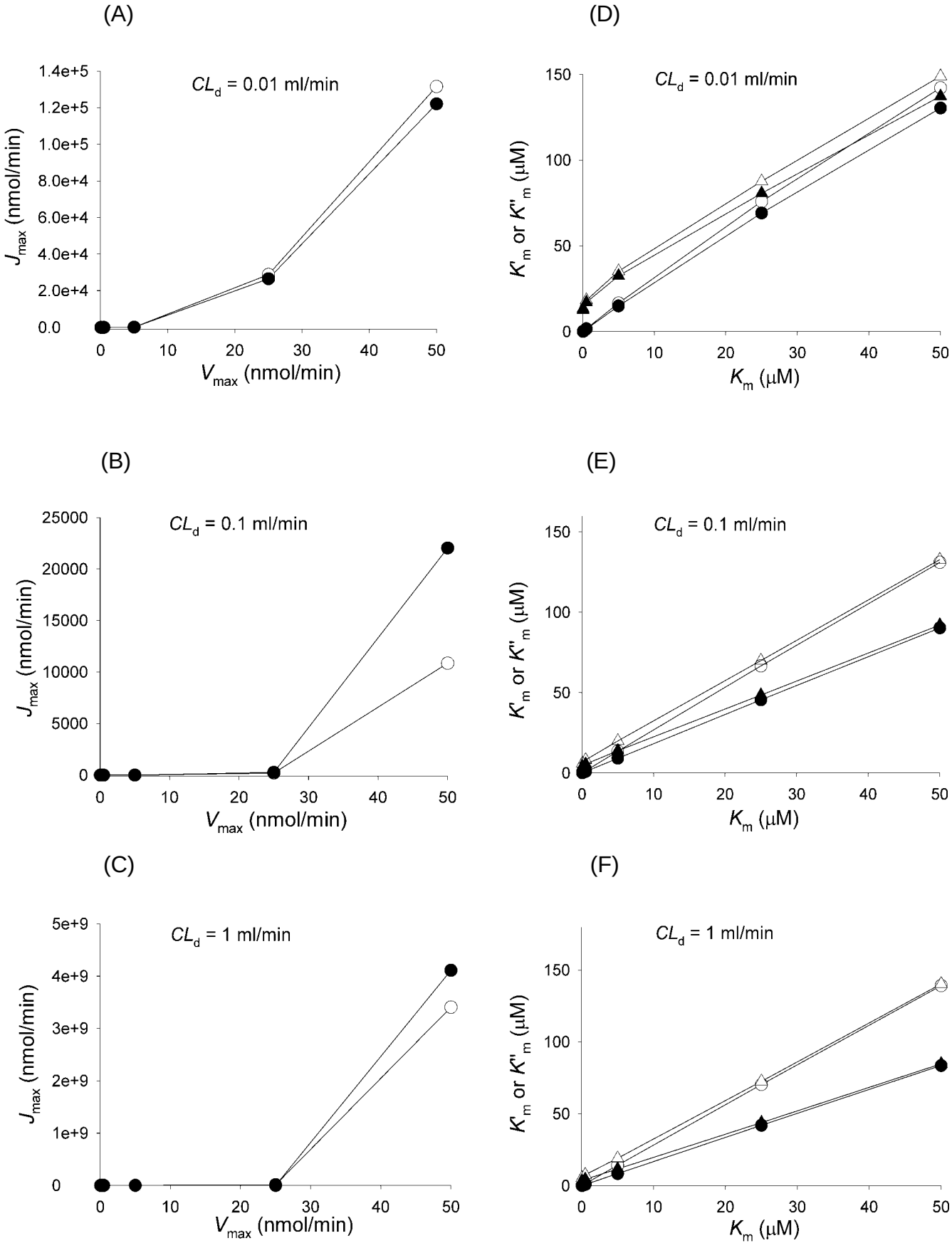

Figure 15

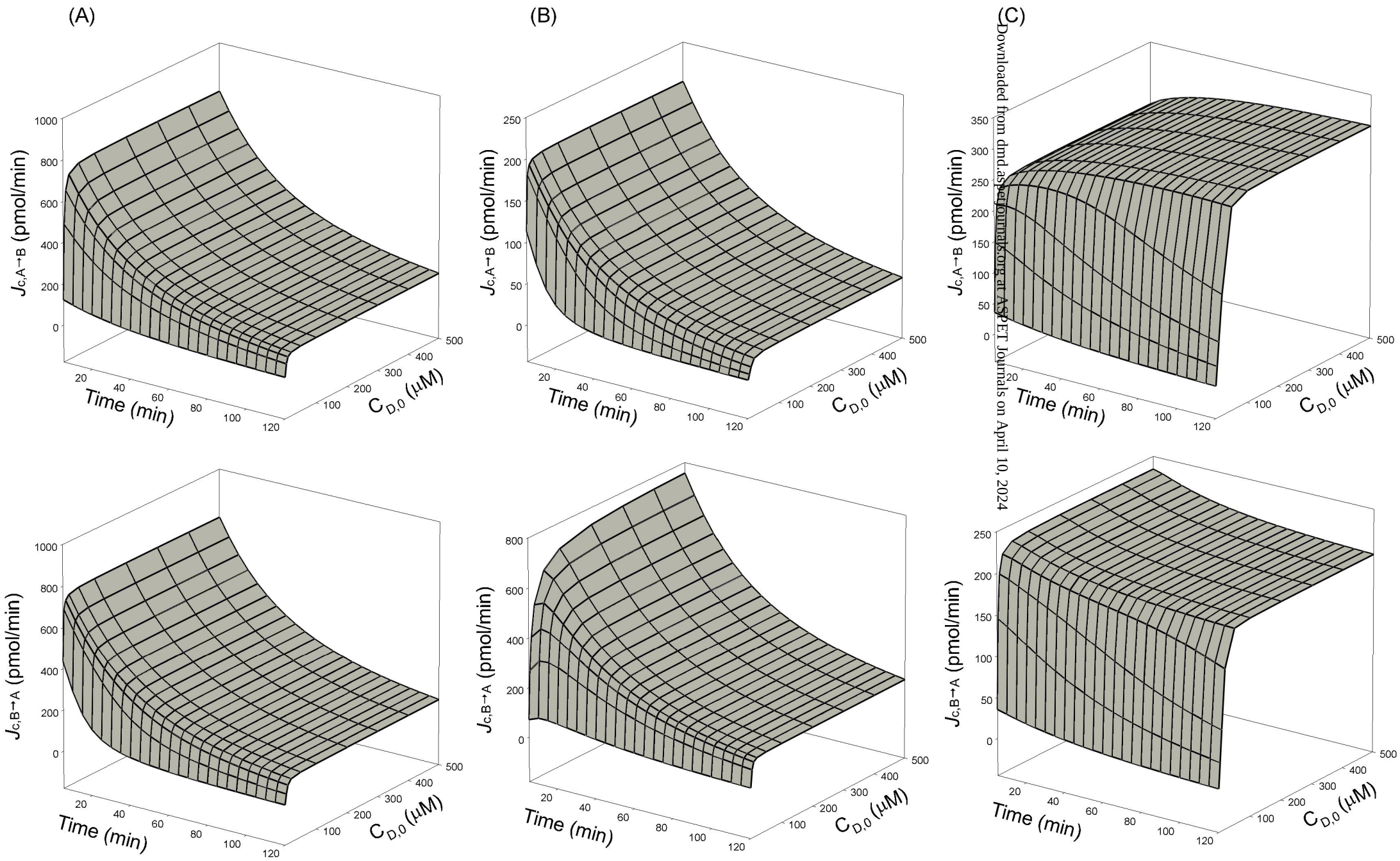

DMD Fast Forward. Published on October 11, 2007 as DOI: 10.1124/dmd.107.015321
This article has not been copyedited and formatted. The final version may differ from this version.

Figure 16

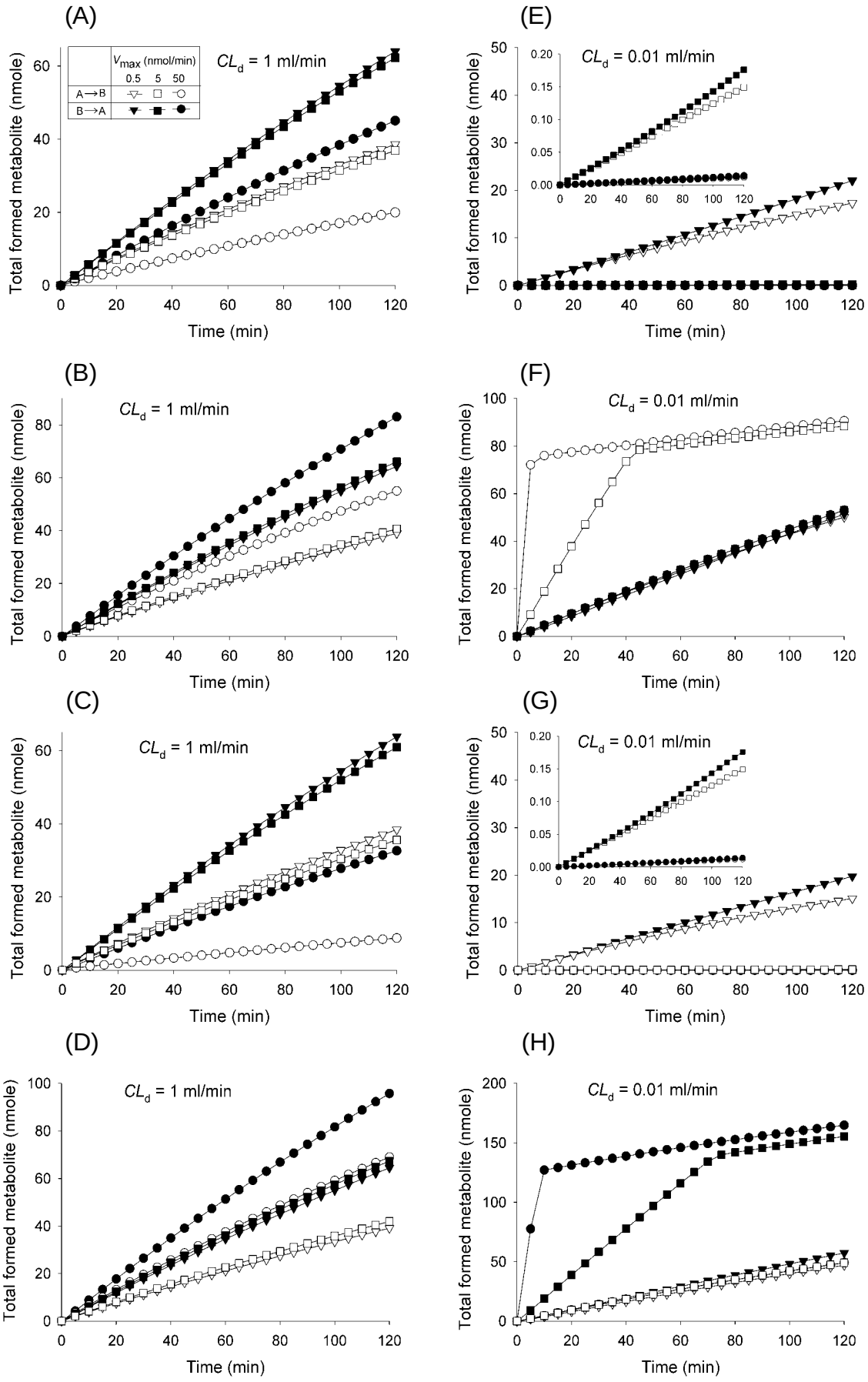

DMD Fast Forward. Published on October 11, 2007 as DOI: 10.1124/dmd.107.015321
This article has not been copyedited and formatted. The final version may differ from this version.

Figure 17

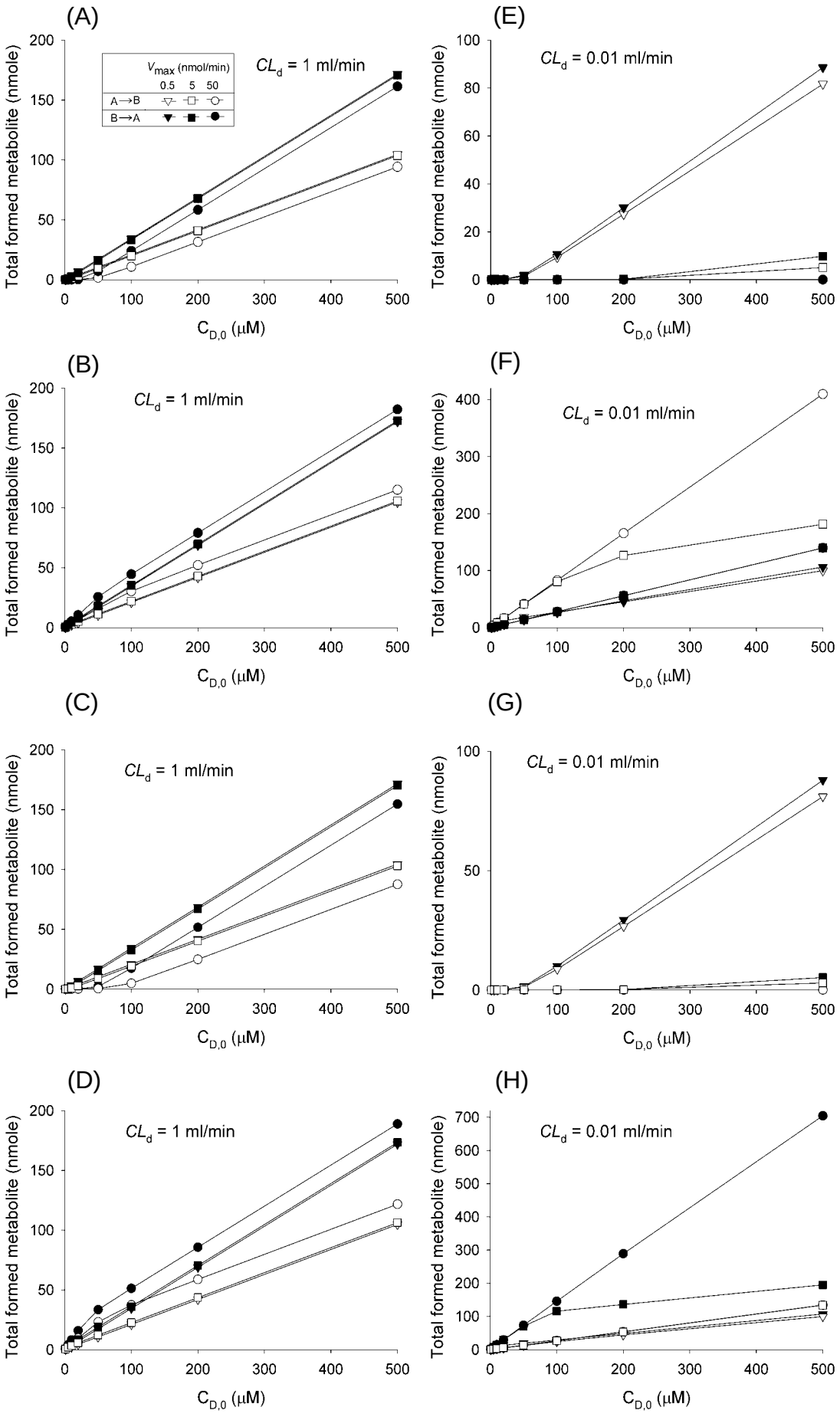

DMD Fast Forward. Published on October 11, 2007 as DOI: 10.1124/dmd.107.015321
This article has not been copyedited and formatted. The final version may differ from this version.

Figure 18

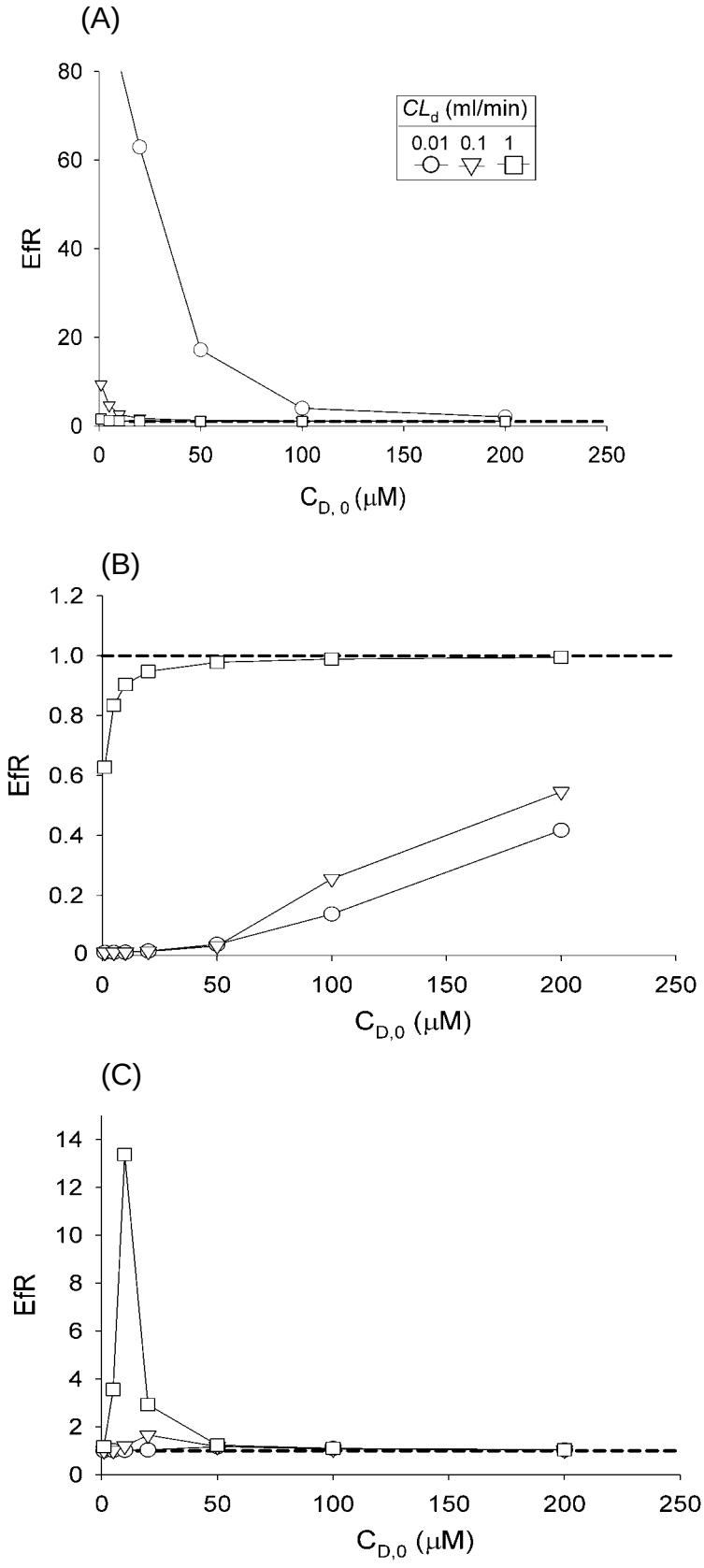

DMD Fast Forward. Published on October 11, 2007 as DOI: 10.1124/dmd.107.015321
This article has not been copyedited and formatted. The final version may differ from this version.

APPENDIX

Mass Balance Equations in Caco-2 cell monolayer for linear conditions

In apical compartment

$$V_{ap}\frac{dC_{ap}}{dt}=-(CL_{abs}+CL_{d4})f_{ap}C_{ap}+(CL_{int,sec}+CL_{d3})f_{cell}C_{cell} \quad (A1)$$

In cellular compartment

$$V_{cell}\frac{dC_{cell}}{dt}=(CL_{abs}+CL_{d4})f_{ap}C_{ap}+(CL_{d1}+CL_{influx})f_{baso}C_{baso} - (CL_{int,sec}+CL_{d3}+CL_{int,met}+CL_{d2}+CL_{efflux})f_{cell}C_{cell} \quad (A2)$$

In basolateral compartment

$$V_{baso}\frac{dC_{baso}}{dt}=(CL_{d2}+CL_{efflux})f_{cell}C_{cell}-(CL_{d1}+CL_{influx})f_{baso}C_{baso} \quad (A3)$$

Mass Balance Equations in caco-2 cell monolayer for non-linear conditions:

For saturation of apical secretion,

In the apical compartment:

$$V_{ap}\frac{dC_{ap}}{dt}=-(CL_{abs}+CL_{d4})f_{ap}C_{ap}+\left(\frac{V_{max}}{K_m+f_{cell}C_{cell}}+CL_{d3}\right)f_{cell}C_{cell} \quad (A4)$$

In the cellular compartment:

$$V_{cell}\frac{dC_{cell}}{dt}=(CL_{abs}+CL_{d4})f_{ap}C_{ap}+(CL_{d1}+CL_{influx})f_{baso}C_{baso} - \left(\frac{V_{max}}{K_m+f_{cell}C_{cell}}+CL_{d3}+CL_{int,met}+CL_{d2}+CL_{efflux}\right)f_{cell}C_{cell} \quad (A5)$$

In the basolateral compartment:

$$V_{baso}\frac{dC_{baso}}{dt}=(CL_{d2}+CL_{efflux})f_{cell}C_{cell}-(CL_{d1}+CL_{influx})f_{baso}C_{baso} \quad (A6)$$

For saturation of apical absorption,

In the apical compartment:

DMD Fast Forward. Published on October 11, 2007 as DOI: 10.1124/dmd.107.015321
This article has not been copyedited and formatted. The final version may differ from this version.

$$V_{ap}\frac{dC_{ap}}{dt}=-\left(\frac{V_{max}}{K_m+f_{ap}C_{ap}}+CL_{d4}\right)f_{ap}C_{ap}+\left(CL_{int,sec}+CL_{d3}\right)f_{cell}C_{cell} \quad (A7)$$

In the cellular compartment:

$$V_{cell}\frac{dC_{cell}}{dt}=\left(\frac{V_{max}}{K_m+f_{ap}C_{ap}}+CL_{d4}\right)f_{ap}C_{ap}+\left(CL_{d1}+CL_{influx}\right)f_{baso}C_{baso}-\left(CL_{int,sec}+CL_{d3}+CL_{int,met}+CL_{d2}+CL_{efflux}\right)f_{cell}C_{cell} \quad (A8)$$

In the basolateral compartment

$$V_{baso}\frac{dC_{baso}}{dt}=\left(CL_{d2}+CL_{efflux}\right)f_{cell}C_{cell}-\left(CL_{d1}+CL_{influx}\right)f_{baso}C_{baso} \quad (A9)$$

For saturation of cellular metabolism

$$V_{ap}\frac{dC_{ap}}{dt}=-\left(CL_{abs}+CL_{d4}\right)f_{ap}C_{ap}+\left(\frac{V_{max}}{K_m+f_{cell}C_{cell}}+CL_{d3}\right)f_{cell}C_{cell} \quad (A10)$$

In the cellular compartment:

$$V_{cell}\frac{dC_{cell}}{dt}=\left(CL_{abs}+CL_{d4}\right)f_{ap}C_{ap}+\left(CL_{d1}+CL_{influx}\right)f_{baso}C_{baso}-\left(CL_{int,sec}+CL_{d3}+\frac{V_{max}}{K_m+f_{cell}C_{cell}}+CL_{d2}+CL_{efflux}\right)f_{cell}C_{cell} \quad (A11)$$

In the basolateral compartment

$$V_{baso}\frac{dC_{baso}}{dt}=\left(CL_{d2}+CL_{efflux}\right)f_{cell}C_{cell}-\left(CL_{d1}+CL_{influx}\right)f_{baso}C_{baso} \quad (A12)$$